

# Evolution in the Disks and Bulges of Group Galaxies since $z = 0.4$

Sean L. McGee<sup>1</sup>, Michael L. Balogh<sup>1</sup>, Robert D. E. Henderson<sup>1</sup>, David J. Wilman<sup>2</sup>, Richard G. Bower<sup>3</sup>, John S. Mulchaey<sup>4</sup>, Augustus Oemler Jr.<sup>4</sup>

<sup>1</sup>Department of Physics and Astronomy, University of Waterloo, Waterloo, Ontario, N2L 3G1, Canada

<sup>2</sup>Max-Planck-Institut für extraterrestrische Physik, Giessenbachstrasse 85748 Garching Germany

<sup>3</sup>Department of Physics, University of Durham, Durham, UK, DH1 3LE

<sup>4</sup>Observatories of the Carnegie Institution of Washington, 813 Santa Barbara Street, Pasadena, California, USA

17 April 2008

## ABSTRACT

We present quantitative morphology measurements of a sample of optically selected group galaxies at  $0.3 < z < 0.55$  using the *Hubble Space Telescope (HST)* Advanced Camera for Surveys (ACS) and the GIM2D surface brightness-fitting software package. The group sample is derived from the Canadian Network for Observational Cosmology Field Redshift survey (CNOC2) and follow-up Magellan spectroscopy. We compare these measurements to a similarly selected group sample from the Millennium Galaxy Catalogue (MGC) at  $0.05 < z < 0.12$ . We find that, at both epochs, the group and field fractional bulge luminosity (B/T) distributions differ significantly, with the dominant difference being a deficit of disk-dominated ( $B/T < 0.2$ ) galaxies in the group samples. At fixed luminosity,  $z=0.4$  groups have  $\sim 5.5 \pm 2$  % fewer disk-dominated galaxies than the field, while by  $z=0.1$  this difference has increased to  $\sim 19 \pm 6$  %. Despite the morphological evolution we see no evidence that the group environment is actively perturbing or otherwise affecting the entire existing disk population. At both redshifts, the disks of group galaxies have similar scaling relations and show similar median asymmetries as the disks of field galaxies. We do find evidence that the fraction of highly asymmetric, bulge-dominated galaxies is  $6 \pm 3$  % higher in groups than in the field, suggesting there may be enhanced merging in group environments. We replicate our group samples at  $z = 0.4$  and  $z = 0$  using the semi-analytic galaxy catalogues of Bower et al. (2006). This model accurately reproduces the B/T distributions of the group and field at  $z=0.1$ . However, the model does not reproduce our finding that the deficit of disks in groups has increased significantly since  $z=0.4$ .

**Key words:** galaxies: evolution, galaxies: formation, galaxies:structure

## 1 INTRODUCTION

Galaxies, at a simple level, are a mixture of two fundamental and distinct components: a bulge and a disk. In the local universe, bulge dominated galaxies are generally red and quiescent, while disk dominated galaxies are generally blue and actively forming stars (Blanton et al. 2003). Thus, the morphology of galaxies may be important when trying to explain the observations that show the cosmic star formation density has rapidly declined from a peak at  $z \sim 1.5$  (Lilly et al. 1996; Madau et al. 1996; Hopkins 2004), and that the fraction of red galaxies has rapidly increased over the same time (Faber et al. 2007; Bell et al. 2004). Indeed, these observations suggest that the process which transforms

galaxies from disk-dominated to bulge-dominated is also the process which transforms them from the blue cloud to the red sequence (eg., Bell et al. 2007). However, studies of red, disk-dominated galaxies (Wolf et al. 2005) and blue, bulge-dominated galaxies (Abraham et al. 1991; Menanteau et al. 2006) suggest this model may be too general. In addition, the large fractions of passive spirals at intermediate redshift suggests that the truncation of star formation may happen before the morphological transformation mechanism (Poggianti et al. 1999, but see Wilman et al. 2008).

The local environment of a galaxy is an important factor in its evolution. Observations of galaxy clusters have shown that galaxies within clusters have lower star formation rates than the general field (eg. Balogh et al. 1999).

The rapid structure growth associated with  $\Lambda$ CDM cosmology, which increases the local galaxy density of the average galaxy with time, may be the key driver of the decline of galaxy star formation rates. Indeed, analogous to the lower star formation rates in clusters, there is a correlation between the local galaxy surface density and the morphology of galaxies (Dressler 1980). At low redshift, the percentage of early type galaxies increases, and the percentage of late types decreases, with increasing density. Interestingly, Dressler (1980) found that this relation was equally strong in centrally-concentrated, relaxed clusters and in irregular, less centrally-concentrated clusters. At higher redshift,  $z \sim 0.5$ , Dressler et al. (1997) showed that this *morphology-density relation* is stronger in highly concentrated clusters than in less concentrated clusters.

Although these studies point to the crucial role clusters play in the morphological transformation of galaxies, they are rare environments, and thus cannot have a large enough effect on the properties of galaxies to explain the decline of the star formation density of the universe as a whole. However, the less dense environment of optically selected groups is the most common environment for galaxies in the local universe (Eke et al. 2004). Indeed, Postman & Geller (1984) found that the morphology-density relation extends smoothly into the group scale environments. Further supporting the integral role of groups, suppressed galaxy star formation rates in group-scale environments of the local universe is now well-established (eg., Balogh et al. 2004). Wilman et al. (2005a) have shown that the fraction of galaxies with  $[\text{OII}]\lambda 3727\text{\AA}$  emission, a measure of star formation, is much higher in group galaxies at intermediate redshift,  $z \sim 0.4$ , than in the local universe; however, the group galaxies still exhibit suppressed star formation relative to the field at the same epoch.

The physical cause of the suppression of star formation since  $z \sim 1$  isn't clear, but there are many candidates, each with their own morphological signatures. Within the context of  $\Lambda$ CDM cosmology, galaxy mergers are often thought to be a dominant mechanism (Hopkins et al. 2007). Simulations suggest that a major merger between two gas-rich and star-forming spiral galaxies produces a gas-poor, passively evolving elliptical galaxy (Toomre & Toomre 1972; Mihos & Hernquist 1996). If dominant, this scenario suggests that quiescent spiral galaxies should be rare, and that the transformation of morphological type should precede or happen at the same time as the complete suppression of star-formation. Group environments are thought to be the ideal place for galaxy mergers because of their high density and small relative velocities.

Recently, driven by dual observations of large bubbles seen in the hot X-ray gas of the intracluster medium (McNamara et al. 2000; Fabian et al. 2000) and the correlation between the mass of the galactic bulge and the size of the central supermassive black hole (Magorrian et al. 1998; Ferrarese & Merritt 2000), feedback from active galactic nuclei has become a popular explanation for the suppression of star formation rates in massive galaxies. Semi-analytic galaxy formation models have successfully introduced these mechanisms in a parametrised way (Bower et al. 2006; Croton et al. 2006), but the details are still uncertain. Such energy feedback mechanisms may not directly alter the

galaxy morphology, but reduced star formation may result in significant fading of the disk component.

Meaningful morphological measurements are necessary to break the degeneracy of physical explanations of star formation truncation. Visual classification of galaxies onto a Hubble (or similar) system has proven to be very useful for the study of galaxy evolution. However, the high resolution and uniform quality of large galaxy surveys has given rise to automated morphology systems which attempt to make more quantitative measurements than a visual system will allow. Non-parametric morphology systems (eg. Abraham et al. 2003; Lotz et al. 2004) are robust, but are not easily linked to physical quantities such as bulge or disk scale lengths. For this reason, in this paper we use a popular code, GIM2D (Simard et al. 2002), to fit parametric models to the surface brightness profiles. Parametric systems suffer because they fit an *a priori* model to the galaxy surface brightness and, as such, are prone to giving non-physical results in some cases. We therefore adopt the logical filtering system proposed by Allen et al. (2006), to help mitigate some of these effects.

In this paper, we examine the morphological properties of optically selected samples of group galaxies at  $z=0.4$  and  $z=0.1$ . In §2 we describe our data samples and our morphological measurements. In §3 we present the main data results and in §4 we discuss what the data tells us about galaxies in transformation and compare our data results with the semi-analytic galaxy catalogue of Bower et al. (2006). We summarize our main results in §5. Details of the group-finding algorithm are given in Appendix A, while in Appendix B we consider possible systematic effects on our results. Finally, in Appendix C we show a representative sample of images from our CNOC2  $z=0.4$  sample of galaxies. Throughout this paper we assume a cosmology with matter density  $\Omega_m = 0.3$ , energy density  $\Omega_\Lambda = 0.7$ , and present-day Hubble constant  $H_0 = 100h \text{ km s}^{-1} \text{ Mpc}^{-1}$  with  $h = 0.75$  (or  $h_{75} = 1$ ).

## 2 THE DATA

### 2.1 The $0.3 \leq z \leq 0.55$ Sample

Our moderate-redshift galaxy sample is derived from the Canadian Network for Observational Cosmology Field Galaxy Redshift Survey (CNOC2), a spectroscopic and photometric survey completed with the Multi-Object Spectrograph instrument at the 3.6-m Canada France Hawaii telescope (Yee et al. 2000). The survey was designed to study galaxy clustering and evolution. It targeted galaxies in the redshift range  $0.1 < z < 0.6$  over four different patches of sky totaling about 1.5 square degrees. The survey consists of 5 colour (U,B,V,R<sub>C</sub>, I<sub>C</sub>) photometry of  $\sim 40,000$  galaxies to a limiting magnitude of  $R_C = 23.0$  mag. Spectroscopic redshifts of  $\sim 6000$  galaxies were obtained with an overall sampling rate of 48% to  $R_C = 21.5$ . This large survey allowed Carlberg et al. (2001) to identify a set of 200 groups using a friends-of-friends redshift-space group finder.

Wilman et al. (2005b) followed the CNOC2 survey with deeper spectroscopy of a set of 26 groups (20 targeted, 6 serendipitous) drawn from the Carlberg et al. catalogue using the Low Dispersion Survey Spectrograph (LDSS2) at the 6.5m Baade telescope at Las Campanas Observatory in

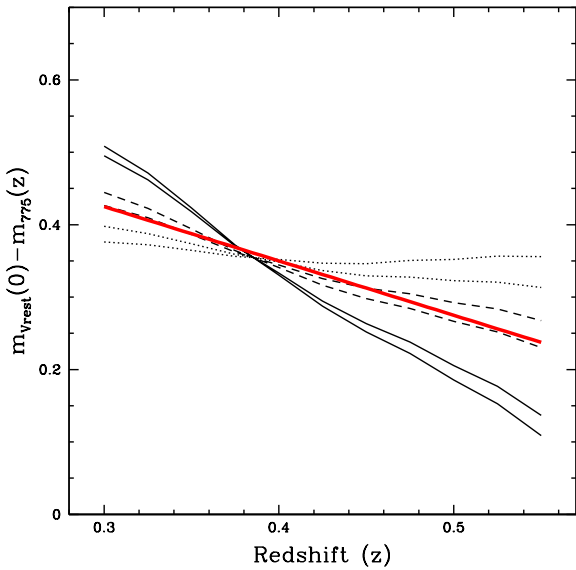


**Figure 1.** We show k-corrections to rest frame V band magnitudes, derived from a suite of Bruzual & Charlot (2003) population synthesis models. The solid lines indicate a constant star formation rate; the dashed lines are models with an exponentially declining star formation rate; and the dotted lines represent single stellar population models created at  $z = 4$ . All models are shown with and without one magnitude of dust extinction. The thick red line indicates the adopted k-correction of  $k' = -0.75 z + 0.65$ .

Chile. These groups were chosen to lie within  $0.3 < z < 0.55$ , and galaxies brighter than  $R_C = 22.0$  were targeted for spectroscopy. This additional spectroscopy was designed to give near full completeness at bright magnitudes ( $R_C < 20$ ; for details, see Wilman et al. 2005b).

For each of the 20 targeted groups, we obtained single orbit *Hubble Space Telescope (HST)* Advanced Camera for Surveys (ACS) pointings in the F775W filter during Cycle 12. These data were processed with the ACS pipeline as described by Pavlovsky et. al (2005). The images were further processed with the *Multidrizzle* task in *pyraf* to remove cosmic rays and hot pixels.

Sources were detected in the *HST* ACS images using the SExtractor software v2.3.2 (Bertin & Arnouts 1996). For a source to be accepted, the signal in at least 10 of its ACS pixels ( $0.5 \text{ arcsec}^2$ ) had to be a minimum of  $1.3 \sigma$  above the background. The faintest sources that are reliably detected using these criteria have  $R_{775} \approx 23.9$ . In this paper we restrict the analysis to sources with redshifts ( $R_C < 22$ ) and are therefore insensitive to these detection parameters. However, we are sensitive to the deblending parameters as the automated surface brightness fits use the segmentation image produced by SExtractor to identify which pixels belong to the galaxy. We used 32 deblending subthresholds, with a minimum contrast parameter of  $9.0 \times 10^{-4}$ . By trial and error, these parameters gave the best deblending upon visual inspection of the output segmentation images.

We have used a suite of Bruzual & Charlot (2003) population synthesis models to k-correct our *HST* magnitudes. We have chosen to avoid large k-corrections by correcting all galaxies to the nearest restframe waveband,  $V$ . Figure 1

shows the models used. The k-correction is mainly sensitive to the star formation history and dust attenuation of the galaxy, and is insensitive to the initial mass function and the metallicity. We add a correction of  $k' = -0.75 z + 0.65$ , shown by the red dashed line, to each of our galaxies. This was chosen to minimize bias for any single galaxy type, but dominates the uncertainty in the magnitudes to  $\pm 0.1$ . In all cases, our statistical uncertainties dominate over this source of systematic error. All *HST* magnitudes are quoted in the k-corrected rest frame  $V$  band.

### 2.1.1 The Group and Field Samples

The group catalogue of Carlberg et al. (2001) originally identified virialized galaxy groups in redshift space using an iterative friends-of-friends algorithm on the CNOC2 redshift catalog. They found over 200 groups, with an average of 3.8 confirmed members per group. To take advantage of the deeper and more complete LDSS2 spectroscopy available to us, we redefine the CNOC2 groups following Wilman et al. (2005b). We discuss the group finding algorithm in more detail in Appendix A. Briefly, an iterative procedure is used, which initially selects galaxies within two times the velocity dispersion of the mean group redshift, and with a transverse distance from the group centre within  $1/5$  of the dispersion distance. In each iteration, the velocity dispersion is recomputed using the Gapper estimator (Beers et al. 1990) and the centre is recomputed as the luminosity-weighted geometric centre of the group. The iterations are continued until a stable group membership is reached.

Using these group centers and velocity dispersions, we restrict the membership of our group sample to galaxies within two velocity dispersions of the group redshift and within  $500h_{75}^{-1}\text{kpc}$  of the group center in the transverse direction. To obtain a true sample of group-sized halos we further restrict our group sample to have velocity dispersions  $< 700 \text{ km/s}$  within  $500h_{75}^{-1}\text{kpc}$  of the group center.

Field samples of galaxies are commonly defined in one of two ways: as an “isolated” sample, in which galaxies within groups and clusters are removed, or as a “global” sample, which includes all galaxies regardless of their environment. In practice, the removal of all group and cluster galaxies is not possible in our sample. Incomplete redshift sampling and the observational uncertainties associated with group membership would lead to an “isolated” field sample which still contained some group galaxies. Therefore, we prefer to define a field sample that contains all galaxies, regardless of their group or cluster membership. However, our follow-up spectroscopy focused on regions that have groups identified in the CNOC2 survey, and our morphologies are derived from small ACS images centered on each of 20 targeted groups. To avoid the bias toward groups that would otherwise be present, we define our field sample to include only those galaxies that are not in groups as identified by the Carlberg et al. algorithm. As discussed in §2.2.1 and Appendix A, because of the incompleteness of the CNOC2 survey, and the strict group finding algorithm of Carlberg, this leaves a field sample which is only slightly depleted in group galaxies when compared to the universe as a whole at  $z=0.4$ . A similar selection in the semi-analytic group catalogues discussed later (§4.3) shows that the field sample will have only  $\sim 8\%$  fewer group galaxies than a true global field sample.

We could correct for this bias by creating a true field sample which is an admixture made of 92% observed field sample and 8% group sample. However, all of our conclusions are insensitive to this correction, and for the sake of simplicity, we do not apply it to our results.

Using these definitions yields a sample of 114 group galaxies and 128 field galaxies with  $0.3 \leq z \leq 0.55$  and  $M_V < -19$ .

## 2.2 The $z \sim 0.1$ Sample

Our sample of low redshift galaxies is derived from the Millennium Galaxy Catalog (MGC). The MGC is a 37.5 square degree B-band imaging survey carried out using the Wide Field Camera on the Isaac Newton Telescope (Liske et al. 2003). The survey is a long, 35 arcmin wide strip, fully contained within both the Two Degree Field Galaxy Redshift Survey (2dFGRS) and the Sloan Digital Sky Survey (SDSS). The photometric catalogs are complete to  $B < 24$  mag, and the imaging is of sufficient quality to allow for the decomposition of galaxies into a bulge and disk component.

MGCz, the redshift survey component of the MGC, was designed to obtain AAT/2dF spectra of  $B < 20$  galaxies which were not covered by either 2dFGRS or SDSS (Driver et al. 2005). This gives a redshift completeness of 96% for  $B < 20$  galaxies.

### 2.2.1 The Group and Field Samples

There exist many low redshift group catalogues derived from either the SDSS or 2dF surveys. However, we wish to create a catalogue that can be compared directly and fairly with our higher-redshift group sample. The latter was derived from a two-step process — the initial survey and the targeted group follow-up — applied to an incomplete redshift survey. This method is not the most direct or efficient way to find groups in our lower-redshift sample, but it does accurately reproduce our higher-redshift selection and the possible biases within. We discuss the method in detail in Appendix A. Briefly, we reduce the completeness of the low redshift sample to match the sampling rate of the CNOC2 survey, and then reproduce the Carlberg et al. (2001) algorithm. To mimic our follow-up of Carlberg et al. (2001) groups, we then increase the completeness and recompute the group membership.

Using this method we have found 19 groups with velocity dispersions between 100 km/s and 700 km/s and which lie in the range  $0.06 < z < 0.12$ . Using a volume-limited sample of  $M_B < -18$ , we have a sample containing 99 group members and 3022 field galaxies. As discussed in § 2.1.1, a true field sample would contain all group members and field galaxies. However, to maintain consistency between the CNOC2 and MGC samples we do not exclude the small number of group galaxies from our field sample. In practice, due to the size of the field sample ( $\sim 3000$ ), adding or removing the 99 group galaxies has no effect on the bulk properties of the field.

The low percentage of galaxies in groups in our sample seems in contradiction with other group catalogues based on local redshift surveys. For example, the 2dF Percolation Inferred Galaxy Groups (2PIGG) catalogue (Eke et al.

2004), which is based on the 2dF survey, finds that  $\sim 55\%$  of galaxies are in groups in the local universe. However, the fraction of 2PIGG groups with more than two members and within velocity dispersion limits of 100 km/s to 700 km/s (which are our criteria) is only 24%. The reduction of the sampling rate to match the CNOC2 completeness results in the non-detection of about half of these groups. A further 30% of galaxies are not found in groups because the Carlberg algorithm is not a strict friends-of-friends procedure: there is an additional step to check that candidate group galaxies are overdense with respect to the background. Accounting for these selection effects, we would only expect to find 9 % of galaxies satisfying our definition of a group. Finally, we also remove groups which are not fully contained within the very narrow MGC strip, i.e. the group centers are within  $500h_{75}^{-1}$  kpc of a survey edge. This step reduces the volume from which groups are selected from by  $\sim 30\%$ . Our group catalogue is therefore incomplete relative to 2PIGG, but our sample is robust (see §4.3.1) and accurately reproduces the CNOC2 group-finding algorithm at higher redshift. The small number of group galaxies confirms, as suggested in §2.1.1, that our field sample is only slightly depleted in group galaxies when compared to the Universe as whole. Indeed, our results are unchanged if we include these group galaxies in our field population at this redshift, but for consistency with the CNOC2 groups, we do not.

## 2.3 Comparison of Surveys

The measurement of a galaxy's morphology can depend on a number of factors besides its intrinsic morphology, such as the imaging wavelength, angular resolution and surface brightness limit. Because of these systematic differences, direct measurement of morphological evolution is difficult. In this paper, we largely concentrate on a direct comparison between group and field galaxies at fixed redshift, which eliminates the effects of these systematic differences. Nonetheless, the MGC and CNOC2 are quite well matched in the key areas, which allows us to compare the differential group and field behavior between redshifts.

Specifically, the two surveys probe approximately the same restframe wavelength. The MGC survey is a rest frame B Band (observed frame  $\sim 440$  nm) survey, while our ACS images are in the rest frame V Band (observed frame  $\sim 775$  nm). Since disks tend to be bluer than bulges one might expect a lower B/T when measured in the B-band; however the intrinsic morphological differences are only significant at much wider wavelength separation (Taylor-Mager et al. 2007).

The apparent surface brightness limit of the MGC survey is 26 mag/arcsec<sup>2</sup> and that of the *HST* ACS images is 30 mag/arcsec<sup>2</sup>. Figure 2 shows the absolute surface brightness limits of the two surveys as a function of redshift, including  $(1+z)^4$  cosmological dimming. For the redshift ranges of interest, the absolute surface brightness limits are comparable.

The excellent angular resolution of our *HST* ACS images (point spread function (PSF) FWHM  $\sim 0.1$  arcsec) allows for morphological measurements of the CNOC2 sample. In fact, this gives a physical resolution which is somewhat better than the MGC survey (PSF FWHM  $\sim 1$  arcsec) in the redshift range of interest, as shown in Figure 3. Of

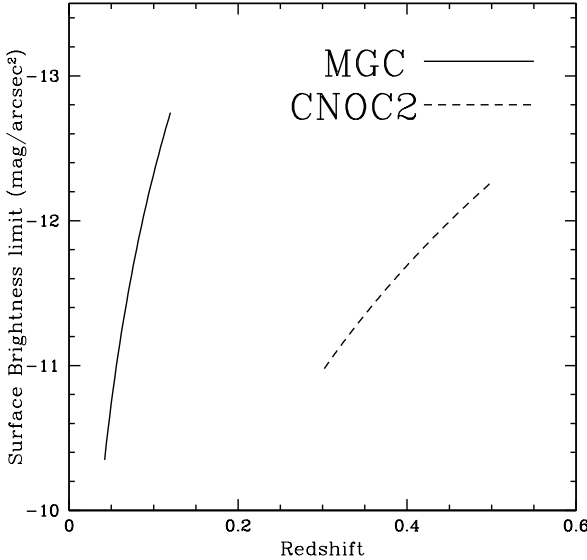


**Figure 2.** A comparison of the absolute surface brightness limits of our two samples of galaxies, as function of redshift. The solid line represents the MGC surface brightness (26 mag/arcsec<sup>2</sup>), while the dashed line is the equivalent for the CNOC2 sample (30 mag/arcsec<sup>2</sup>).

greater concern is that the physical PSF of the MGC survey has a large variation within the sample itself, due to the redshift range spanned by the galaxies. In Appendix B, we investigate the effect of the physical resolution on the morphological measurements. We find that the resolution differences have no effect on the bulge-to-total light measurements, but do affect the asymmetry parameter, causing the measured asymmetry to be higher in galaxies with better resolution. In this paper, we only analyze asymmetry measures on matched samples of galaxies, which mitigates this effect.

The properties of galaxies vary with luminosity (eg., Baldry et al. 2004), so when comparing morphological properties between the two surveys we must use a common luminosity limit. Fukugita et al. (1995) have shown that late type galaxies (Scd to Sab) have B-V=0.5–0.78, while early type galaxies (S0 and E) have B-V=0.85–0.96. Thus, our  $z = 0.4$  magnitude limit of  $M_V < -19$  corresponds approximately to an MGC limit between  $M_B = -18.5$  and  $-18.0$ , depending on type and neglecting any luminosity evolution. Therefore, when directly comparing the group and field behavior between the two surveys we only consider MGC galaxies brighter than  $M_B \approx -18$  (except in Figure 5 which includes galaxies as faint as  $M_B = -16$ ).

#### 2.4 Gim2d Morphological Measurements

Allen et al. (2006) have presented morphological measurements of the MGC and we follow their procedure to derive morphological parameters for the CNOC2 sample. We use the parametric IRAF package GIM2D (Simard et al. 2002; Marleau & Simard 1998), which fits the sky-subtracted surface brightness distribution of each galaxy with up to 12 parameters describing a bulge and a disk component.

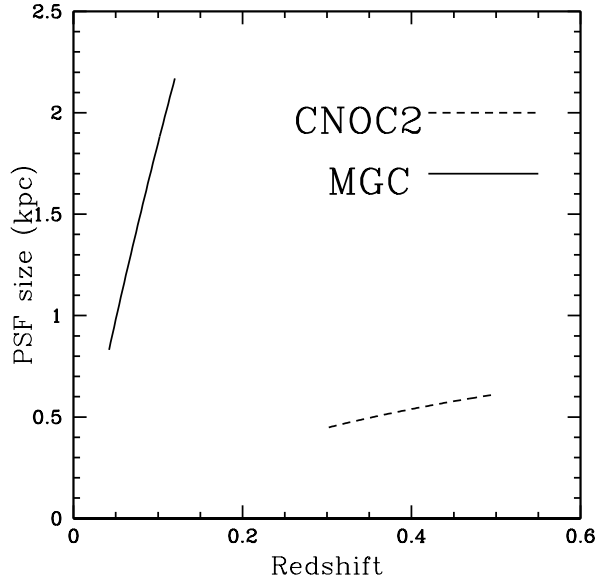


**Figure 3.** A comparison of the point spread function FWHM of our two samples of galaxies as a function of redshift. The solid line represents the ground-based MGC PSF (1 arcsec), while the dashed line corresponds to the *HST* resolution of the higher redshift CNOC2 sample (0.1 arcsec).

GIM2D searches the large-parameter space of models using a Metropolis et al. (1953) algorithm, which is inefficient but does not easily get trapped in local minima. Häussler et al. (2007) have shown that GIM2D produces reliable fits with small systematic errors when the effective galaxy surface brightness is above the sky level, as it is for the galaxies in our sample.<sup>1</sup>

The GIM2D algorithm can fit single component (Sersic profile) or two component (Sersic + exponential disk) models to the galaxy profile. The Sersic profile is given by

$$I_b(R) = I_e \exp \left[ -b_n [(R/R_e)^{1/n} - 1] \right], \quad (1)$$

where  $I_e$  is the intensity at the radius,  $R_e$ , and  $n$  is the Sersic index. The parameter  $b_n$  is set to  $1.9992n - 0.3271$  within GIM2D to ensure that  $R_e$  is the projected radius which encloses half the total luminosity.

In a two component fit, the Sersic profile corresponds to the bulge model, and the disk is fit by an exponential model,

$$I_d(R) = I_0 \exp(-R/h), \quad (2)$$

where  $I_0$  is the central intensity,  $I_d(R)$  is the disk light profile as a function of radius  $R$ , and  $h$  is the scale length.

Ideally, we would like to fit two components to all galaxies, but often galaxies do not have two resolvable components. It is for this reason that we follow the prescription

<sup>1</sup> Häussler et al also show that another parametric galaxy fitting code, GALFIT (Peng et al. 2002), performs better than GIM2D in crowded fields. However, GALFIT uses a downhill gradient algorithm which, although very efficient, may not be as robust as the simulated annealing technique of GIM2D for problems with many local minima, like two-component fitting.

of Allen et al. (2006), who have made a careful study of GIM2D output. They suggest a logical filtering system which initially fits a two-component model to the galaxy. For galaxies which have “normal” light profiles, this fit is kept, but for those galaxies which have perturbed profiles or are obviously better described by a single component, we fit a pure Sersic profile. In practice, this has little effect on our results.

#### 2.4.1 Residual Substructure

To quantify the substructure in the surface brightness profiles we use the residual parameter,  $R$ , as defined by Schade et al. (1995). This parameter is also known as the “asymmetry parameter,  $R$ ” (Im et al. 2002) and the “residual substructure parameter,  $S$ ” (McIntosh et al. 2004). It is defined as

$$R = R_T + R_A \quad (3)$$

with

$$R_T = \frac{\Sigma(|R_{ij} + R_{ij}^{180}|/2)}{\Sigma I_{ij}} - \frac{\Sigma(|B_{ij} + B_{ij}^{180}|/2)}{\Sigma I_{ij}} \quad (4)$$

$$R_A = \frac{\Sigma(|R_{ij} - R_{ij}^{180}|/2)}{\Sigma I_{ij}} - \frac{\Sigma(|B_{ij} - B_{ij}^{180}|/2)}{\Sigma I_{ij}} \quad (5)$$

where  $R_T$  is the total residual parameter and  $R_A$  is the asymmetric residual parameter.  $R_{ij}$  is the flux at pixel position (i,j) in the residual image,  $R_{ij}^{180}$  is the flux at (i,j) in the residual image rotated by  $180^\circ$ .  $B_{ij}$  and  $B_{ij}^{180}$  are the corresponding values in the background noise. Finally,  $I_{ij}$  is defined as the flux at (i,j) in the object image. The sum is done over all pixels out to  $r = 2r_{hl}$ , where  $r_{hl}$  is the radius at which half the galaxy’s light is enclosed.

### 3 RESULTS

Although our data sample is comprised of a relatively large number of group galaxies (99 in the MGC sample and 114 in the CNOC2 sample), each group has typically less than ten spectroscopically confirmed members. Therefore, we stack the individual groups to maximize the signal of the bulk group galaxy properties. Weinmann et al. (2006) have shown that the velocity dispersion of a group is a poor tracer of the mass of the group halo, especially for groups containing few confirmed members. Although our group velocity dispersions vary from 100 km/s to 700 km/s, Wilman et al. (2005b) has shown that the individual CNOC2 groups show no significant differences based on group type or velocity dispersion from a combined group. Thus we combine all the galaxies within  $500h_{75}^{-1}$  kpc of a group center at each redshift to form a stacked  $z \sim 0.1$  group and a stacked  $z \sim 0.4$  group. Because of the large uncertainties on the velocity dispersions we do not attempt to estimate a “virial radius” for each group, but instead simply require a group member to be within  $500h_{75}^{-1}$  kpc of the group center, corresponding approximately to the expected virial radius of a typical group in our sample, with a 360 km/s velocity dispersion.

#### 3.1 B/T Distribution

In Figure 4, we present the quantitative morphology distribution of the two samples. We compare field and group distributions of the ratio of the bulge luminosity to total luminosity (B/T) of each galaxy. Pure bulge galaxies have a B/T of 1, while pure disk galaxies have a B/T of 0. The left hand panel of Figure 4 shows the B/T distribution for the  $z \sim 0.4$  sample of galaxies. The red line represents the stacked group from the CNOC2 sample and the black line represents the field galaxies. A Kolmogorov-Smirnov (KS) test shows that the group and field sample are not drawn from a common parent distribution, with 98.4% confidence. The most significant difference within the CNOC2 sample is at  $B/T < 0.2$ , where the fraction of galaxies in the field ( $\sim 57 \pm 5\%$ ) is higher than that in groups ( $\sim 41 \pm 5\%$ ). In the right hand panel of Figure 4, we present the B/T distribution for the  $z \sim 0.1$  sample. Similar to the CNOC2 sample, the fraction of  $B/T < 0.2$  galaxies is much higher in the field ( $\sim 54 \pm 1\%$ ) than in the groups ( $\sim 32 \pm 6\%$ ). A KS test rules out a common origin for the group and field distributions of the MGC sample at greater than 99.9 % confidence.

In both plots we have seen evidence for the well-known morphology-density relation. In this case, it is manifested as a deficit of disk dominated galaxies in the group samples when compared to the field. However, it is known that bright galaxies tend to be more frequently bulge-dominated than faint galaxies. Therefore, it is possible that this form of the morphology-density relation is related to different field and group luminosity distributions rather than any intrinsic difference between group and field galaxies at fixed luminosity. To explore this we present Figure 5, which shows the fraction of disk-dominated galaxies as a function of total galaxy magnitude. Studies of the B/T distribution of visually classified galaxies have shown that elliptical and S0 galaxies predominately have  $B/T > 0.3-0.4$  (Tran et al. 2001 and Wilman et al. 2008), but we chose to define “disk dominated” to indicate galaxies with  $B/T < 0.2$ . This choice is made to isolate those galaxies in the bin with the most significant difference between the group and field samples, but our conclusions are unchanged even if we use  $B/T < 0.4$  to define disk-dominated galaxies.

The left hand panel of Figure 5 shows the  $z \sim 0.4$  sample, with the thick black line representing field galaxies and the thin red line representing the groups. In any one luminosity bin there is no significant difference (ie.  $> 1\sigma$ ) between the fraction of disk galaxies in the group and field; however, overall there is a systematic difference of  $5.5 \pm 2\%$ , in the sense that the fraction of disk-dominated galaxies in groups is always lower than in field galaxies of comparable luminosity.

The right hand panel of Figure 5 shows the disk fraction as a function of magnitude for the  $z \sim 0.1$  sample. The magnitude is the rest frame B band, the waveband in which the B/T decomposition was done. In this figure, we show all galaxies in our redshift range to  $M_B = -16$ , fainter than our volume-limited sample of  $M_B < -18$ . The dashed vertical line indicates the equivalent B-band limit of the CNOC2  $M_V = -19$  magnitude limit, assuming a B-V color of 0.63, which is typical of a late-type galaxy (Fukugita et al. 1995). At this redshift there is clearly a significant difference in the

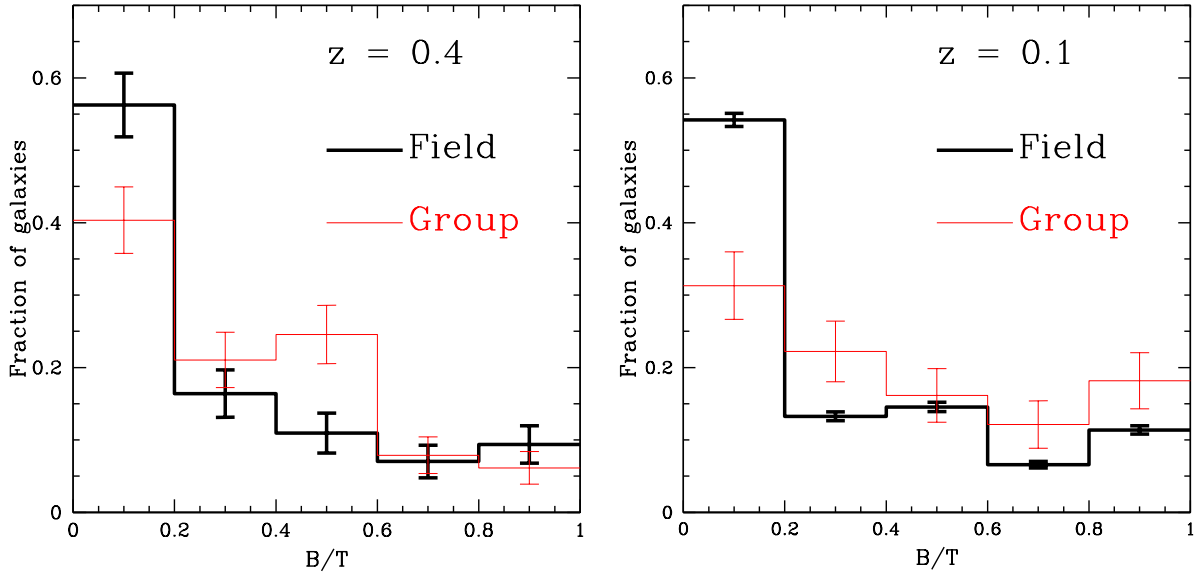


**Figure 4.** The histogram of relative bulge luminosity for the  $z \sim 0.4$  (left) and  $z \sim 0.1$  (right) samples. The thin red line in each plot indicates the stacked group at that redshift, and the thick black line is the field sample. Uncertainties are estimated with the jackknife technique.

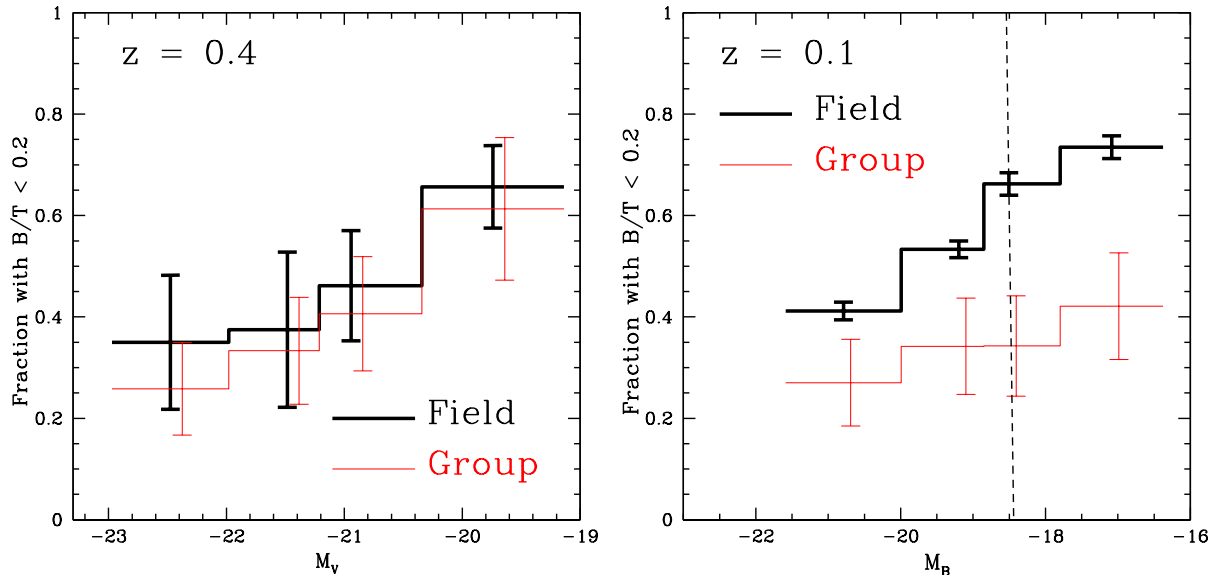


**Figure 5.** The fraction of galaxies with  $B/T < 0.2$  (disk-dominated) as a function of absolute magnitude. Left: The  $z \sim 0.4$  sample. Magnitudes are measured using the flux calculated by GIM2D and k-corrected to rest frame V band. Right: The  $z \sim 0.1$  sample, where magnitudes are measured in the B band. The field galaxies are represented by the thick black line and the group galaxies by the thin red line. The dashed vertical line indicates the equivalent B-band limit corresponding to the CNOC2  $M_V = -19$  magnitude limit, assuming a B-V color of 0.63. Uncertainties are measured using the jackknife technique.

fraction of disk-dominated systems between group and field galaxies of the same luminosity. This difference is  $24 \pm 6\%$  over the full magnitude range of the sample, and  $19 \pm 6\%$  brighter than the equivalent CNOC2 luminosity limit.

Although the B/T distributions of the group and field galaxies are different at both redshifts, this predominately reflects a difference in luminosity distributions at high redshifts, but an intrinsic difference in the fraction of disk galaxies of fixed luminosity at low redshift. It therefore appears

that the morphological segregation in groups has increased significantly from  $z \sim 0.4$  to  $z \sim 0.1$ . We recall that the  $z=0.1$  sample is measured in the rest frame B band while the  $z=0.4$  sample is measured in the rest frame V band. It would be possible to mimic our results if the disks of group galaxies were significantly redder than the disks of field galaxies. However, to create a B-band disk fraction consistent with the V band disk fraction, the disks of group galaxies must be B-V=2.07 redder than the disks of field galaxies. On aver-

age, in the MGC sample, pure disk ( $B/T=0$ ) group galaxies are only  $B-V=0.01$  redder than the pure disk field galaxies. Thus, it appears the evolution is real. We will further explore the colours of these galaxies, including a comparison with the CNOC2 sample, in a future paper.

### 3.2 Structural Parameters

The evolution in morphological segregation suggests there is a change occurring within the group galaxies between  $z \sim 0.4$  and  $z \sim 0.1$ . Here we focus on the possible causes of this evolution. We first look for structural differences between the group and field galaxies. If star formation in group galaxies is quenched, then the disk of the galaxy may slowly fade away, and we might expect to see a departure from the normal scaling relations between disk size and luminosity.

In Figure 6 we plot the distribution of disk magnitudes as a function of the disk scalelength, excluding only the most bulge-dominated galaxies ( $B/T > 0.7$ ).<sup>2</sup> The left hand panel shows the  $z \sim 0.4$  sample, while the right hand panel shows the  $z \sim 0.1$  sample. In both plots it is evident that there is a correlation between the disk size and its brightness, such that brighter disks have larger disk scale lengths. This is not surprising, but the fact that the group and field lie on the same relation (although with large scatter) is. The thick solid black line is the best fit to the scaling relation of the field galaxies. Best fit lines are determined using a robust biweight estimator which minimizes the effect of distant outliers. In principle, uniform fading of a perfectly exponential disk would result in a lower disk luminosity, but would leave the scalelength unchanged.<sup>3</sup> Therefore, an ideal population of faded disk galaxies would exhibit the same scaling relation, but with different normalization. Adopting this assumption, we fit only the normalization to the group galaxy relation, while maintaining the slope defined by the field galaxies, as shown by the thin red line. There is no statistically significant difference between the normalizations of the group and field populations (a difference of  $0.086 \pm 0.134$  for the  $z=0.4$  sample, and  $0.103 \pm 0.151$  for the  $z=0.1$  sample).

Since we do not see any significant difference in the disk scaling relations for group galaxies, it may be that the process of morphological transformation is instead dominated by a growing bulge (for example, through mergers). Again, if this were true, we might expect to see a deviation in the group and field bulge scaling relations. In Figure 7, we plot the distribution of bulge magnitudes as a function of the bulge half light radius, excluding the most disk-dominated galaxies ( $B/T < 0.3$ ). The left hand panel shows the  $z \sim 0.4$  sample and the right hand panel has the  $z \sim 0.1$  sample.

<sup>2</sup> An occasional problem in modeling the surface brightness profile of galaxies with automated programs is the tendency to fit small disk (or bulge) components to galaxies which may have (e.g.) twisted isophotes. Thus we restrict our analysis to galaxies which have significant disk (or bulge) components when looking at their scaling properties.

<sup>3</sup> Häussler et al. (2007) have shown that the recovered scale length is underestimated for low S/N galaxies which are fit with a Sersic profile. However, our data are sufficiently deep to avoid this problem, typically reaching the surface brightness limiting isophotal radius at 3-5 disk scale lengths.

The field and group distributions are again similar, at both redshifts. In §4, we examine the constraints these findings place on the amount of fading which is possible in the group sample.

### 3.3 Asymmetry

In this section we examine the asymmetries of the galaxies, to try to untangle a merger-driven transformation scenario from a gradual disk fading model. Galaxy mergers and harassment often produce noticeable asymmetric features, like tidal tails, which could manifest themselves as deviations from the smooth surface brightness profiles we have used for the morphological measurements. If galaxy mergers were enhanced in groups, we would expect to see an increase in the fraction of galaxies with large asymmetries. On the other hand, the cessation of star formation in the disk would likely result in the disappearance of bright clumps and spiral arms, thereby removing residual substructure, making the disks appear smoother.

We have seen that the fraction of disk galaxies depends on magnitude, and that the difference in the high redshift  $B/T$  distribution is partly due to different luminosity distributions in the field and group samples. For this reason, in the rest of this section, we match the field and group luminosity and redshift distributions. In the MGC sample, we match each group galaxy to the field galaxy with the closest magnitude and within 0.03 in redshift. The magnitude differences for these matched galaxies are all less than 0.02 because of the large number of available field galaxies in the sample. Similarly, for the CNOC2 sample, we match group galaxies to the nearest field galaxy in magnitude (within 0.2 mags) and within 0.05 in redshift. We match all 99 group galaxies in the MGC and 105 of the 114 CNOC2 group galaxies. The brightest CNOC2 group galaxies have no field counterpart, and so are effectively excluded from the remainder of this analysis.

To probe the substructure of the galaxies, we have calculated the asymmetry parameter according to the definitions given in §2.4.1. In Figure 8 we show the distribution in asymmetry for bulge dominated ( $B/T > 0.5$ ) and disk dominated ( $B/T < 0.5$ ) galaxies for both the CNOC2 and MGC surveys. The dashed vertical line indicates the lower limit for “highly asymmetric” galaxies ( $R_T + R_A > 0.16$ ), as defined by Patton et al. (2005). Disk dominated galaxies have much higher median asymmetries than bulge dominated galaxies, as expected. However, there is no appreciable difference in the median asymmetry between the group and luminosity-matched field, in any of the samples. Although we can not resolve the disappearance of individual HII regions, visual inspection of disk dominated galaxies in Figures C1 and C2 clearly show that galaxies with low  $B/T$  and high asymmetries have strong asymmetric structures typical of star forming galaxies, ie. large spiral arms and lumpy regions. The lack of a systematic difference in the asymmetries of matched group and field disk-dominated galaxies means that we find no evidence for a mechanism that suppresses star formation in group disks.

We note that, as shown in Figure 3, the CNOC2 sample has a lower physical PSF than the MGC sample. We show in Appendix B that galaxies which are blurred to have a lower physical resolution have lower asymmetry values. Therefore,

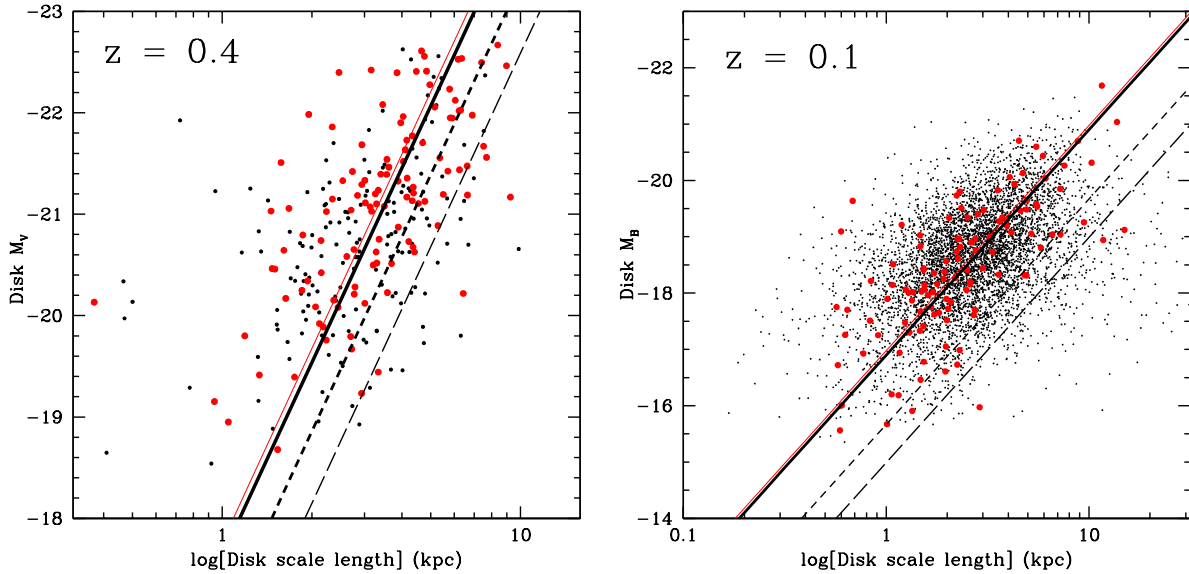


**Figure 6.** The distribution of disk magnitudes as a function of disk scalelength for non-bulge dominated galaxies ( $B/T < 0.7$ ). Left:  $z \sim 0.4$  sample. Right:  $z \sim 0.1$  sample. Large red points are group galaxies and small, black points are field galaxies. The thick solid black line is the best fit to the field, thin red line is the group best fit. The dotted (dashed) black line shows the effect of truncating star formation 1(3) Gyrs ago.

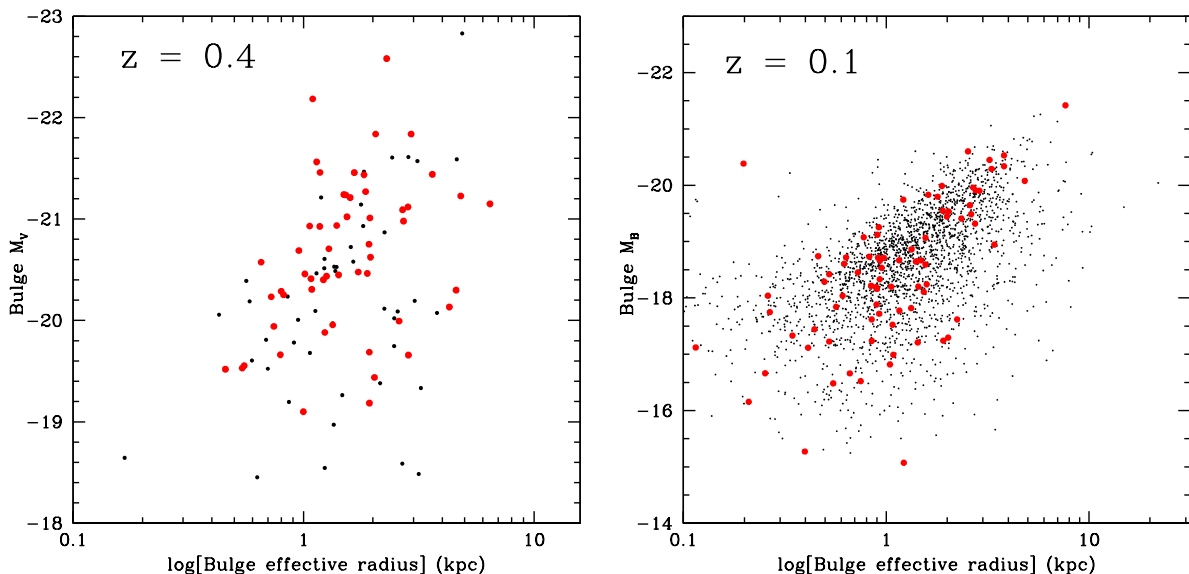


**Figure 7.** The distribution of bulge magnitude as a function of bulge half light radius for non-disk dominated ( $B/T > 0.3$ ) galaxies. Left: The  $z \sim 0.4$  sample. Large, red points are group galaxies and small, black points are field galaxies. Right: The  $z \sim 0.1$  sample. Red, filled points are group galaxies and black points are field galaxies.

we do not consider the change in median asymmetry between  $z \sim 0.4$  and  $z \sim 0.1$  as evidence of real evolution.

## 4 DISCUSSION

### 4.1 Galaxies in Transformation?

In this section we investigate how our results in §3 might constrain the number galaxies that are in the process of

transforming within the group environment. Specifically, we have shown in §3.2 that the bulge- and disk-components appear to obey scaling relations between size and luminosity that are independent of environment. This suggests that any transformation mechanism must either leave these scaling laws intact, or only affect a small number of galaxies at the epoch of observation. To investigate this, we consider a simple Bruzual & Charlot (2003) model with a constant star formation rate as appropriate for the disk components. If this star formation is suddenly truncated, within 1 Gyr it

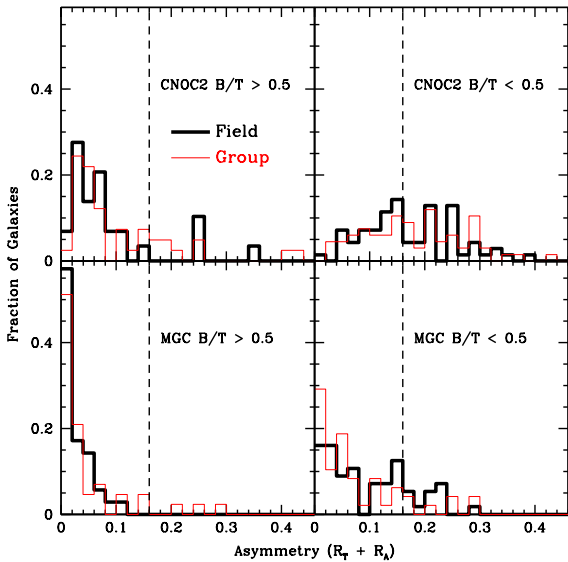


**Figure 8.** The distribution of asymmetries ( $R_T + R_A$ ) for CNOC2 bulge dominated galaxies (top left), CNOC2 disk dominated galaxies (top right), MGC bulge dominated galaxies (bottom left), and MGC disk dominated galaxies (bottom right). In all plots group galaxies are represented by the thin red line and the luminosity matched field is the thick black line. The dashed vertical line indicates the lower limit for “highly asymmetric” galaxies ( $R_T + R_A > 0.16$ ) as defined by Patton et al. (2005).

will have subsequently faded by 1.23 magnitudes in rest-*B* (as measured for the MGC sample), or 0.68 magnitudes in rest-*V* (appropriate for the higher-*z* CNOC2 sample). After 3 Gyr, the amount of fading expected is 1.91 mags (B) or 1.39 mags (V). However, such truncation should not affect the measured scale length of the disk. Therefore, if star formation were truncated in the entire population of group galaxies, we would expect the normalization of the scaling relation to change by these amounts. These relations are shown by the dotted (1 Gyr) and dashed (3 Gyr) black lines in Figure 6. These lines are significantly offset from the measured group relation (which is consistent with that of the field); therefore, we can easily rule out that star formation has been recently truncated in the entire disk population.

We would next like to establish what *fraction* of group galaxies could have undergone 1 (3) Gyr fading and still have a scaling relation that is consistent with the observed field scaling relation (ie.  $< 2\sigma$  difference in the normalization, corresponding to a difference of 0.2 magnitudes for the MGC sample, and 0.18 magnitudes for CNOC2). To assess this we randomly choose a sample of group galaxies from Figure 6 and fade their disks for 1 (3) Gyrs according to the Bruzual & Charlot model described above. We recompute the B/T ratios of the sample, and impose our selection criteria on total magnitude and B/T (recall we are excluding the most bulge-dominated galaxies from this analysis). The normalization of the scaling relation is then refit to the new set of data, keeping the slope fixed. We can then determine an upper limit on the fraction of galaxies which may have undergone such fading for 1 (3) Gyrs; these limits are  $41 \pm 3\%$  ( $29 \pm 4\%$ ) for the CNOC2 sample, and  $9 \pm 3\%$

( $4 \pm 2\%$ ) for the MGC sample. The upper limit for the  $z=0.4$  sample is quite high, as expected given the relatively small sample size. Therefore, based on these data alone, we cannot rule out the hypothesis that a substantial fraction of these galaxies are undergoing a significant change in their star formation rate. The upper limit for the  $z = 0.1$  sample is much more restrictive, partly because of the sample size and partly because the rest-frame B-band is more sensitive to recent star formation. Our limits mean that any mechanism able to truncate star formation in disks is not dominant in present day groups.

Mergers are likely to be rare, but transformative events, so an increased merger history in groups would not be expected to increase the median asymmetry of group galaxies, but rather increase the fraction of highly asymmetric galaxies. By examining the fraction of galaxies with  $R_T + R_A > 0.16$ , we see that an extra  $\sim 6 \pm 3\%$  of group galaxies are highly asymmetric in the bulge-dominated samples at both redshifts, compared with the matched field sample (8). The fraction of highly asymmetric galaxies in the disk-dominated samples is similar for both the group and the luminosity-matched field. This may indicate that there is an increase of merging or interacting galaxies in groups. A visual inspection of the CNOC2 galaxies shows that 4 out of 9 of the “high-asymmetry” bulge dominated galaxies are indeed merging or interacting, as shown in Appendix C.

## 4.2 A comparison with X-ray selected groups

In §3.3, we have shown that the median asymmetry of group and field galaxies are statistically indistinguishable. These results are interesting because Tran et al. (2001) have shown that, in a sample of local X-ray selected groups, there is evidence for smoother disks in group galaxies than in the field. Studies of blue cluster galaxies have also shown that they have significantly lower asymmetry values than their blue field counterparts (McIntosh et al. 2004). Perhaps most intriguingly, Homeier et al. (2006) has recently shown that X-ray luminous clusters have galaxies with significantly lower average asymmetries than X-ray faint clusters. A related difference from our results comes from studies of X-ray group galaxy morphology, which have shown that the fraction of early types is  $\sim 0.7$  (Mulchaey et al. 2006; Jeltema et al. 2007) in the same magnitude and redshift range as our CNOC2 sample. To compare our data with this number we define early-type galaxies as those with  $B/T > 0.4$ , as Tran et al. (2001) has shown that this provides a good match with early type galaxies as classified on the Hubble-sequence. Using this definition, we find an early-type fraction of only  $\sim 46\%$  in the CNOC2 group sample, considerably lower than found in X-ray groups at this redshift. We will revisit this issue in a future paper when we consider and compare the results of Hubble-sequence morphological classification (Wilman et al. 2008). These results, combined with our result that the median asymmetry in optically selected group galaxies is not different from the luminosity matched field, point to the role that the hot intergalactic medium (IGM) may play in the smoothing of disk galaxies. Alternatively, the progenitors of optically selected groups may be different from the progenitors of X-ray selected ones.

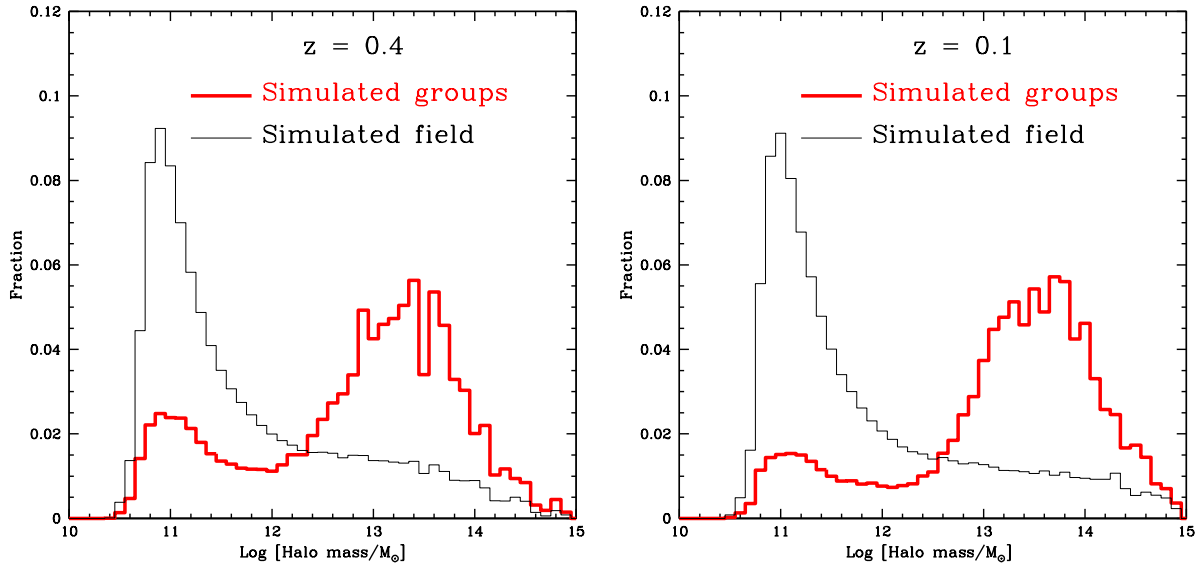


**Figure 9.** The distribution of halo masses for each galaxy in the Bower et al. (2006) model catalogue (thin, black line) and the distributions of galaxy halos in the simulated groups (thick, red line). The high redshift sample is on the left and the low redshift sample is on the right.

#### 4.3 Comparison with semi-analytic galaxy models

Recently, large dark matter simulations of large volumes have allowed theorists to produce usefully large catalogues of model galaxies, employing detailed modeling of galaxy formation based on relatively simple prescriptions for relevant physical processes. In this section we use the catalogues of one such “semi-analytic” galaxy formation model (Bower et al. 2006) to compare with our data. The Bower et al. model uses the dark matter Millennium simulation (Springel et al. 2005), a  $\Lambda$ CDM cosmological box with  $500/h$  Mpc sides, as the basis for the merger trees. The algorithm is based on the earlier GALFORM models of Benson et al. (2003) and Cole et al. (2000). The principal change from the Benson et al. model is a prescription for the quenching of star formation in massive halos by feedback powered by accretion onto a supermassive black hole. However, perhaps the most important change for our purposes is the modification of the method for computing disk instabilities. Disk instabilities are now the dominant mode of bulge formation in these models, although the brightest galaxies are still more often formed through mergers. Unlike older models, morphology is now sensitive to the baryonic physics of disks, rather than the (more robustly-predicted) merger history.

##### 4.3.1 Constructing a mock catalogue

We construct mock catalogues using the Bower et al. (2006) model for the  $z=0.1$  and  $z=0.4$  redshift time steps. Because of the large size of the Millennium simulation and the small spread in redshift of each of our samples, a single simulation box can be used for each epoch. Using the same group-finding procedure as described in detail in Appendix A, we construct a stacked group sample to compare directly with our observations.

In Figure 9, we present the resulting distribution of

galaxy halos in our group sample, compared with all halos in the Millennium simulation. We see that at both redshifts the group-finding algorithm selects predominately galaxies that are in halos with masses  $5 \times 10^{12} < M_{\text{halo}}/M_{\odot} < 10^{15}$ . Both samples peak at  $M_{\text{halo}} \sim 6 \times 10^{13} M_{\odot}$ , but the CNOC2 sample is somewhat biased toward lower masses than the MGC sample. Our algorithm finds a large percentage of groups that are made up principally of large dark matter halos: 76.4 % (85.1 %) of  $z=0.4$  ( $z=0.1$ ) galaxies are in halos with  $M_{\text{halo}} > 10^{12} M_{\odot}$ . In both plots there is a second peak – a distribution of low mass halos – which are contamination. However, we find that 79% ( $z=0.4$ ) and 89% ( $z=0.1$ ) of the  $M_{\text{halo}} < 10^{12} M_{\odot}$  galaxies are within  $500h_{75}^{-1}$  kpc of a galaxy which resides in a halo with  $M_{\text{halo}} > 10^{12} M_{\odot}$ . Thus, the majority of our “contamination” is due to galaxies on the outskirts of a true group. This confirms that the Carlberg et al. (2001) algorithm selects groups which are real, and representative of massive dark matter halos, as also confirmed by previous weak lensing measurements (Parker et al. 2005) and our follow-up spectroscopy (Wilman et al. 2005b). Only 2.5 % (3.1 %) of our  $z=0.4$  ( $z=0.1$ ) galaxies are not associated with a massive ( $M_{\text{halo}} > 10^{12} M_{\odot}$ ) halo.

##### 4.3.2 B/T distribution

In Figure 10, we show the Bower et al. (2006) model predictions for the B/T distributions corresponding to our data samples. In all four panels the data are shown with a thick black line and the model predictions are shown with a thin, dashed, red line. The models are limited at  $M_B < -18$  in the MGC comparisons, and by  $M_v < -19$  for the CNOC2 comparison.

It is clear that there is remarkable agreement between the model and the data at  $z=0.1$ , especially considering that the model does not take into account any observational uncertainties associated with deriving B/T ratios from the sur-

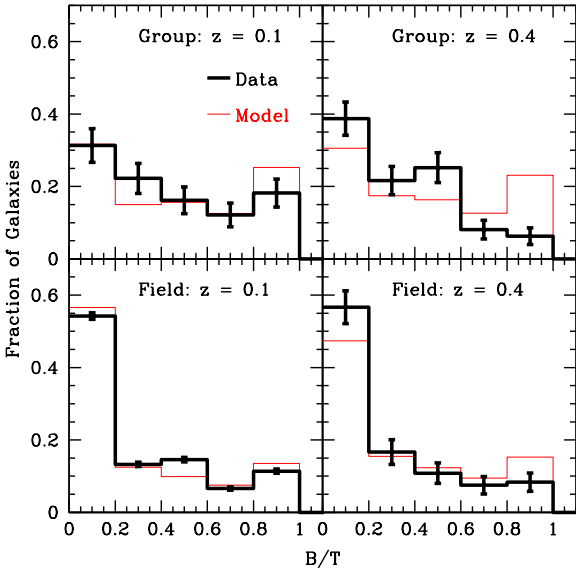


**Figure 10.** The B/T distributions of the Bower et al. (2006) model, compared with the observed group and field samples at  $z=0.1$  and  $z=0.4$ . The model is the thin, red line in each panel and the data is the thick black line.

face brightness profile alone. However, the agreement between the models and the data at  $z=0.4$  is not as good. In particular, the model underpredicts the fraction of  $B/T < 0.2$  galaxies and overpredicts the fraction of  $B/T > 0.8$  galaxies in both the groups and the field. Intriguingly, Figure 10 shows the models also predict that the fraction of disk dominated galaxies increases in the field between  $z=0.4$  and  $z=0.1$ , but remains constant within the groups.

Given these predictions, we are now encouraged to investigate the time evolution of the disk fraction as a function of luminosity. From our data we have seen that the differences in the disk fraction as a function of magnitude are small at  $z=0.4$  ( $\sim 5.5 \pm 2\%$ ), but quite large in the local universe ( $\sim 19 \pm 6\%$ ). To address this, we present Figure 11, which shows the relative disk ( $B/T < 0.2$ ) deficiency between the field and the group samples, as a function of luminosity. The disk deficiency is the difference between the group and field disk fraction divided by the field disk fraction. This gives a measure of the fraction of field disks which are absent at a similar magnitude in the groups. In the left panel of Figure 11 we show the low redshift sample. The data from the MGC sample agrees well on average with the model predictions. In the right panel of Figure 11 we show the same comparison but for the high redshift sample. Although the average value of the group disk deficit is correctly predicted at  $z=0.1$ , the Bower et al. model predicts a group disk deficit which is much higher than the data at  $z=0.4$ . We note that, in the model, the predicted evolution is of a similar magnitude whether measured consistently in rest frame V or rest frame B, indirectly supporting our argument that the observed evolution is not driven by the difference in rest wavelength sampled by the two surveys.

We have seen in Figure 10 that the models underpredict the fraction of  $B/T < 0.2$  at  $z=0.4$  and that this leads to an overprediction of the disk deficiency in groups at the high

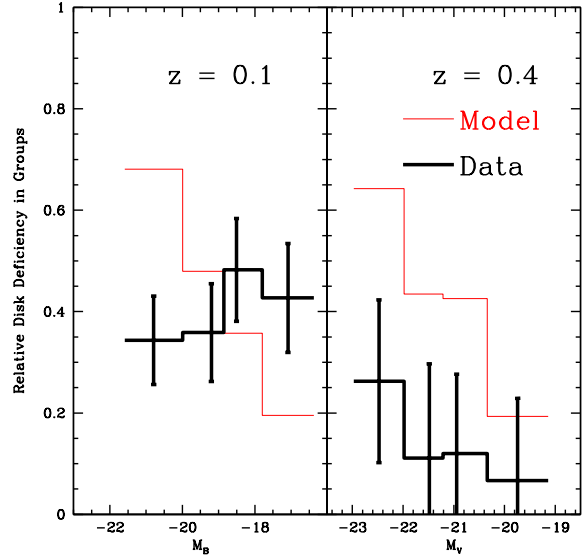


**Figure 11.** The relative disk deficiency in groups, parametrized as 1-group disk fraction/field disk fraction, where a disk has a  $B/T < 0.2$ . This is shown at  $z=0.4$  (right panel) and  $z=0.1$  (left panel) for both the Bower et al model (thin red line) and the data (thick black line).

redshift epoch. Intriguingly, inspection of Figure 10 shows that this is because the models predict that the fraction of disk dominated galaxies increases in the field between  $z=0.4$  and  $z=0.1$ , but remains constant within the groups. While a direct comparison between the two epochs could be complicated by the different observed wavebands, we note that the same model predictions exist when considering only the underlying stellar mass. This is at odds with the data, which show that the  $B/T < 0.2$  fraction *decreases* in the groups, and remains constant in the field.

## 5 CONCLUSIONS

We have presented a quantitative morphology study of optically-selected galaxy groups from two redshift surveys: CNOC2 ( $z \sim 0.4$ ), supplemented with significant additional Magellan spectroscopy, and MGC ( $z \sim 0.1$ ). We have compared these data with a similarly selected sample of groups drawn from the semi-analytic galaxy formation models of Bower et al. (2006). Our findings are:

- There is a significant difference, as indicated by a KS test, in the fractional bulge luminosity ( $B/T$ ) distribution of group and field galaxies, in both the high and low redshift samples. The dominant difference is the deficit of disk-dominated ( $B/T < 0.2$ ) galaxies in the group samples.
- The difference in the disk fraction ( $B/T < 0.2$ ) of group galaxies relative to the field shows significant evolution between  $z=0.4$  and  $z=0.1$ . At a given luminosity in the CNOC2 sample, the groups have  $\sim 5.5 \pm 2\%$  fewer  $B/T < 0.2$  galaxies than the field. By  $z=0.1$  this difference has increased significantly, so that groups have  $\sim 19 \pm 6\%$  fewer  $B/T < 0.2$  galaxies than the field in the same magnitude range. Although the  $z=0.1$  sample traces rest frame B while the  $z=0.4$

sample traces rest frame V, this difference is unlikely to be able to explain the differences.

- At neither redshift do we see any evidence that the bulk properties of the existing disks are significantly different for group galaxies than for field galaxies. They lie on similar scaling relations and show similar asymmetry distributions. There is no evidence that groups are actively perturbing or otherwise affecting a large fraction of the group disk population.

- We find that there is a small enhancement in the fraction of bulge-dominated group galaxies that are highly asymmetric, relative to bulge-dominated galaxies in the field. This may be consistent with enhanced merging in the group environment. Visual inspection of high asymmetry, bulge-dominated CNOC2 galaxies shows that 44% (4/9) exhibit clear evidence of interactions or merging.

- A sample of galaxies drawn from the semi-analytic galaxy catalogues of Bower et al. (2006) was shown to agree remarkably well with the B/T distribution of the field and group galaxies at  $z=0.1$ . However, our data have shown that time evolution of the B/T distributions predicted by the models is not seen in our data. In particular, the Bower et al. model underpredicts the fraction of disk dominated galaxies at  $z \sim 0.4$ .

The morphological difference between group and field galaxies at  $z=0.4$  is mostly due to the tendency for group galaxies to be more luminous and, therefore, more bulge-dominated than field galaxies. This is consistent with our previous findings about group galaxies; namely, that their M/L ratios are consistent with the passive evolution of a predominately old population (Balogh et al. 2007), because the dominant difference in group galaxies is their pre-existing tendency to be bulge-dominated. This is also consistent with the fairly small difference in the emission-line fraction of group and field galaxies, at fixed stellar mass (Balogh et al. 2007) or magnitude (Wilman et al. 2005a).

The failure of the Bower et al. (2006) to reproduce the time evolution of the group disk deficit is interesting. These type of models predict a fairly rapid "strangulation" of galaxies once they enter larger halos, which causes the star formation rate to decrease on timescales of a few Gyr. This starts to play a large role at  $\sim 10^{12}$  solar masses, significantly less massive than most of our groups. Weinmann et al. (2006) have shown that this mechanism is too effective, and produces a homogeneous, red satellite population at all magnitudes, in groups and clusters, which is not observed at  $z=0$ . Gilbank & Balogh (2008) have recently shown that this problem extends out to at least  $z=1$ . It is likely that the incorrect disk deficit evolution is another manifestation of the maximally efficient star formation quenching mechanism used by the models.

We have found that, in contrast to X-ray selected groups, our optically-selected group galaxies have median asymmetries that are similar to field galaxies. This may point to a possible role for galaxy interactions with the hot IGM. Alternatively, the progenitors of X-ray selected group galaxies may be fundamentally different from the progenitors of optically selected group galaxies. X-ray selected groups are more likely to be relaxed, virialized structures, suggesting that they were assembled earlier than optically selected groups. In the current models, the stran-

gulation mechanism is assumed to operate efficiently in small haloes. Thus, little difference is expected in the population of different types of groups many Gyr later (i.e. at the epochs of interest here), since star formation has long ceased in most group members. However, recently it has been suggested that infalling galaxies may be able to retain a significant fraction of their gas (McCarthy et al. 2007; Kawata & Mulchaey 2007), significantly increasing the timescale for star formation to decrease. In this case, the headstart given to galaxies that fall into groups a little earlier may be better able to explain the difference between X-ray and optically selected groups.

## ACKNOWLEDGMENTS

We thank the CNOC2 team for access to their unpublished data and Luc Simard for making GIM2D publicly available. We also thank the GALFORM team for allowing access to the semi-analytic galaxy catalogues. Finally, we thank the MGC team for their data. The Millennium Galaxy Catalogue consists of imaging data from the Isaac Newton Telescope and spectroscopic data from the Anglo Australian Telescope, the ANU 2.3m, the ESO New Technology Telescope, the Telescopio Nazionale Galileo and the Gemini North Telescope. The survey has been supported through grants from the Particle Physics and Astronomy Research Council (UK) and the Australian Research Council (AUS). The data and data products are publicly available from <http://www.eso.org/~jliske/mgc/> or on request from J. Liske or S.P. Driver. MLB acknowledges support from an NSERC Discovery Grant.

## REFERENCES

- Abraham, R. G., Crawford, C. S., & McHardy, I. M. 1991, MNRAS, 252, 482
- Abraham, R. G., van den Bergh, S., & Nair, P. 2003, ApJ, 588, 218
- Allen, P. D., Driver, S. P., Graham, A. W., Cameron, E., Liske, J., & de Propris, R. 2006, MNRAS, 371, 2
- Baldry, I. K., Glazebrook, K., Brinkmann, J., Ivezić, Ž., Lupton, R. H., Nichol, R. C., & Szalay, A. S. 2004, apj, 600, 681
- Balogh, M., Eke, V., Miller, C., Lewis, I., Bower, R., Couch, W., Nichol, R., Bland-Hawthorn, J., Baldry, I. K., Baugh, C., Bridges, T., Cannon, R., Cole, S., Colless, M., Collins, C., Cross, N., Dalton, G., de Propris, R., Driver, S. P., Efstathiou, G., Ellis, R. S., Frenk, C. S., Glazebrook, K., Gomez, P., Gray, A., Hawkins, E., Jackson, C., Lahav, O., Lumsden, S., Maddox, S., Madgwick, D., Norberg, P., Peacock, J. A., Percival, W., Peterson, B. A., Sutherland, W., & Taylor, K. 2004, MNRAS, 348, 1355
- Balogh, M. L., Morris, S. L., Yee, H. K. C., Carlberg, R. G., & Ellingson, E. 1999, ApJ, 527, 54
- Balogh, M. L., Wilman, D., Henderson, R. D. E., Bower, R. G., Gilbank, D., Whitaker, R., Morris, S. L., Hau, G., Mulchaey, J. S., Oemler, A., & Carlberg, R. G. 2007, MNRAS, 374, 1169
- Beers, T. C., Flynn, K., & Gebhardt, K. 1990, AJ, 100, 32

Bell, E. F., Wolf, C., Meisenheimer, K., Rix, H.-W., Borch, A., Dye, S., Kleinheinrich, M., Wisotzki, L., & McIntosh, D. H. 2004, *ApJ*, 608, 752

Bell, E. F., Zheng, X. Z., Papovich, C., Borch, A., Wolf, C., & Meisenheimer, K. 2007, *ApJ*, 663, 834

Benson, A. J., Bower, R. G., Frenk, C. S., Lacey, C. G., Baugh, C. M., & Cole, S. 2003, *ApJ*, 599, 38

Berlind, A. A., Frieman, J., Weinberg, D. H., Blanton, M. R., Warren, M. S., Abazajian, K., Scranton, R., Hogg, D. W., Scoccimarro, R., Bahcall, N. A., Brinkmann, J., Gott, J. R. I., Kleinman, S. J., Krzesinski, J., Lee, B. C., Miller, C. J., Nitta, A., Schneider, D. P., Tucker, D. L., & Zehavi, I. 2006, *ApJS*, 167, 1

Bertin, E. & Arnouts, S. 1996, *A&AS*, 117, 393

Blanton, M. R., Hogg, D. W., Bahcall, N. A., Baldry, I. K., Brinkmann, J., Csabai, I., Eisenstein, D., Fukugita, M., Gunn, J. E., Ivezić, Ž., Lamb, D. Q., Lupton, R. H., Loveday, J., Munn, J. A., Nichol, R. C., Okamura, S., Schlegel, D. J., Shimasaku, K., Strauss, M. A., Vogeley, M. S., & Weinberg, D. H. 2003, *ApJ*, 594, 186

Bower, R. G., Benson, A. J., Malbon, R., Helly, J. C., Frenk, C. S., Baugh, C. M., Cole, S., & Lacey, C. G. 2006, *MNRAS*, 370, 645

Bruzual, G. & Charlot, S. 2003, *MNRAS*, 344, 1000

Carlberg, R. G., Yee, H. K. C., Morris, S. L., Lin, H., Hall, P. B., Patton, D. R., Sawicki, M., & Shepherd, C. W. 2001, *ApJ*, 552, 427

Cole, S., Lacey, C. G., Baugh, C. M., & Frenk, C. S. 2000, *MNRAS*, 319, 168

Croton, D. J., Springel, V., White, S. D. M., De Lucia, G., Frenk, C. S., Gao, L., Jenkins, A., Kauffmann, G., Navarro, J. F., & Yoshida, N. 2006, *MNRAS*, 365, 11

Dressler, A. 1980, *ApJ*, 236, 351

Dressler, A., Oemler, A. J., Couch, W. J., Smail, I., Ellis, R. S., Barger, A., Butcher, H., Poggianti, B. M., & Sharples, R. M. 1997, *ApJ*, 490, 577

Driver, S. P., Liske, J., Cross, N. J. G., De Propris, R., & Allen, P. D. 2005, *MNRAS*, 360, 81

Eke, V. R., Baugh, C. M., Cole, S., Frenk, C. S., Norberg, P., Peacock, J. A., Baldry, I. K., Bland-Hawthorn, J., Bridges, T., Cannon, R., Colless, M., Collins, C., Couch, W., Dalton, G., de Propris, R., Driver, S. P., Efstathiou, G., Ellis, R. S., Glazebrook, K., Jackson, C., Lahav, O., Lewis, I., Lumsden, S., Maddox, S., Madgwick, D., Peterson, B. A., Sutherland, W., & Taylor, K. 2004, *MNRAS*, 348, 866

Faber, S. M., Willmer, C. N. A., Wolf, C., Koo, D. C., Weiner, B. J., Newman, J. A., Im, M., Coil, A. L., Conroy, C., Cooper, M. C., Davis, M., Finkbeiner, D. P., Gerke, B. F., Gebhardt, K., Groth, E. J., Guhathakurta, P., Harker, J., Kaiser, N., Kassin, S., Kleinheinrich, M., Konidaris, N. P., Kron, R. G., Lin, L., Luppino, G., Madgwick, D. S., Meisenheimer, K., Noeske, K. G., Phillips, A. C., Sarajedini, V. L., Schiavon, R. P., Simard, L., Smail, A. S., Vogt, N. P., & Yan, R. 2007, *ApJ*, 665, 265

Fabian, A. C., Sanders, J. S., Ettori, S., Taylor, G. B., Allen, S. W., Crawford, C. S., Iwasawa, K., Johnstone, R. M., & Ogle, P. M. 2000, *MNRAS*, 318, L65

Ferrarese, L. & Merritt, D. 2000, *ApJL*, 539, L9

Fukugita, M., Shimasaku, K., & Ichikawa, T. 1995, *PASP*, 107, 945

Gilbank, D. G. & Balogh, M. L. 2008, *mnras*, L18+

Häussler, B., McIntosh, D. H., Barden, M., Bell, E. F., Rix, H.-W., Borch, A., Beckwith, S. V. W., Caldwell, J. A. R., Heymans, C., Jahnke, K., Jogee, S., Koposov, S. E., Meisenheimer, K., Sánchez, S. F., Somerville, R. S., Wisotzki, L., & Wolf, C. 2007, *apjs*, 172, 615

Homeier, N. L., Postman, M., Menanteau, F., Blakeslee, J. P., Mei, S., Demarco, R., Ford, H. C., Illingworth, G. D., & Zirm, A. 2006, *AJ*, 131, 143

Hopkins, A. M. 2004, *ApJ*, 615, 209

Hopkins, P. F., Bundy, K., Hernquist, L., & Ellis, R. S. 2007, *ApJ*, 659, 976

Im, M., Simard, L., Faber, S. M., Koo, D. C., Gebhardt, K., Willmer, C. N. A., Phillips, A. C., Illingworth, G. D., Vogt, N. P., & Sarajedini, V. L. 2002, *ApJ*, 571, 136

Jeltema, T. E., Mulchaey, J. S., Lubin, L. M., & Fassnacht, C. D. 2007, *ApJ*, 658, 865

Kawata, D. & Mulchaey, J. S. 2007, *ArXiv e-prints*, 707

Lilly, S. J., Le Fevre, O., Hammer, F., & Crampton, D. 1996, *ApJL*, 460, L1+

Liske, J., Lemon, D. J., Driver, S. P., Cross, N. J. G., & Couch, W. J. 2003, *MNRAS*, 344, 307

Lotz, J. M., Primack, J., & Madau, P. 2004, *AJ*, 128, 163

Madau, P., Ferguson, H. C., Dickinson, M. E., Giavalisco, M., Steidel, C. C., & Fruchter, A. 1996, *MNRAS*, 283, 1388

Magorrian, J., Tremaine, S., Richstone, D., Bender, R., Bower, G., Dressler, A., Faber, S. M., Gebhardt, K., Green, R., Grillmair, C., Kormendy, J., & Lauer, T. 1998, *AJ*, 115, 2285

Marleau, F. R. & Simard, L. 1998, *ApJ*, 507, 585

McCarthy, I. G., Frenk, C. S., Font, A. S., Lacey, C. G., Bower, R. G., Mitchell, N. L., Balogh, M. L., & Theuns, T. 2007, *ArXiv e-prints*, 710

McIntosh, D., Rix, H.-W., & Caldwell, N. 2004, *ApJ*, 610, 161

McNamara, B. R., Wise, M., Nulsen, P. E. J., David, L. P., Sarazin, C. L., Bautz, M., Markevitch, M., Vikhlinin, A., Forman, W. R., Jones, C., & Harris, D. E. 2000, *ApJL*, 534, L135

Menanteau, F., Ford, H. C., Motta, V., Benítez, N., Martel, A. R., Blakeslee, J. P., & Infante, L. 2006, *AJ*, 131, 208

Metropolis, N., Rosenbluth, A., Rosenbluth, M., Teller, A., & Teller, E. 1953, *Journal of Chemical Physics*, 21, 1087

Mihos, J. C. & Hernquist, L. 1996, *ApJ*, 464, 641

Mulchaey, J. S., Lubin, L. M., Fassnacht, C., Rosati, P., & Jeltema, T. E. 2006, *ApJ*, 646, 133

Parker, L. C., Hudson, M. J., Carlberg, R. G., & Hoekstra, H. 2005, *ApJ*, 634, 806

Patton, D. R., Grant, J. K., Simard, L., Pritchett, C. J., Carlberg, R. G., & Borne, K. D. 2005, *AJ*, 130, 2043

Pavlovsky et. al, C. 2005, *ACS Data Handbook*, Version 4.0

Peng, C. Y., Ho, L. C., Impey, C. D., & Rix, H.-W. 2002, *AJ*, 124, 266

Poggianti, B. M., Smail, I., Dressler, A., Couch, W. J., Barger, A. J., Butcher, H., Ellis, R. S., & Oemler, A. J. 1999, *ApJ*, 518, 576

Postman, M. & Geller, M. J. 1984, *ApJ*, 281, 95

Schade, D., Lilly, S. J., Crampton, D., LeFèvre, O., Hammer, F., & Tresse, L. 1995, *ApJ*, 451, 1

Simard, L., Willmer, C. N. A., Vogt, N. P., Sarajedini, V. L., Phillips, A. C., Weiner, B. J., Koo, D. C., Im, M.,

Illingworth, G. D., & Faber, S. M. 2002, *ApJS*, 142, 1

Springel, V., White, S. D. M., Jenkins, A., Frenk, C. S., Yoshida, N., Gao, L., Navarro, J., Thacker, R., Croton, D., Helly, J., Peacock, J. A., Cole, S., Thomas, P., Couchman, H., Evrard, A., Colberg, J., & Pearce, F. 2005, *Nature*, 435, 629

Taylor-Mager, V. A., Conselice, C. J., Windhorst, R. A., & Jansen, R. A. 2007, *ApJ*, 659, 162

Toomre, A. & Toomre, J. 1972, *ApJ*, 178, 623

Tran, K.-V. H., Simard, L., Zabludoff, A. I., & Mulchaey, J. S. 2001, *ApJ*, 549, 172

Weinmann, S. M., van den Bosch, F. C., Yang, X., & Mo, H. J. 2006, *MNRAS*, 366, 2

Wilman, D. J., Balogh, M. L., Bower, R. G., Mulchaey, J. S., Oemler, A., Carlberg, R. G., Eke, V. R., Lewis, I., Morris, S. L., & Whitaker, R. J. 2005a, *MNRAS*, 358, 88

Wilman, D. J., Balogh, M. L., Bower, R. G., Mulchaey, J. S., Oemler, A., Carlberg, R. G., Morris, S. L., & Whitaker, R. J. 2005b, *MNRAS*, 358, 71

Wilman, D. J., Pierini, D., Tyler, K., McGee, S. L., Oemler, Jr., A., Morris, S. L., Balogh, M. L., Bower, R. G., & Mulchaey, J. S. 2008, *MNRAS*, accepted, (arXiv/0802.2549)

Wilman et al. 2008, in preparation

Wolf, C., Bell, E. F., McIntosh, D. H., Rix, H.-W., Barden, M., Beckwith, S. V. W., Borch, A., Caldwell, J. A. R., Häussler, B., Heymans, C., Jahnke, K., Jogee, S., Meisenheimer, K., Peng, C. Y., Sánchez, S. F., Somerville, R. S., & Wisotzki, L. 2005, *ApJ*, 630, 771

Yee, H. K. C., Morris, S. L., Lin, H., Carlberg, R. G., Hall, P. B., Sawicki, M., Patton, D. R., Wirth, G. D., Ellingson, E., & Shepherd, C. W. 2000, *APJS*, 129, 475

## APPENDIX A: LOW REDSHIFT GROUP FINDING ALGORITHM

The primary goal of our low redshift group finding algorithm is to reproduce the selection criteria applied to our high redshift groups. Thus, our algorithm is not the most efficient method possible, but it does accurately reproduce our selection and the possible biases within. Further, this method will not result in a complete sample of groups in the MGC strip.

We first find groups in the SDSS main galaxy sample using the original method of Carlberg et al. (2001). The MGC strip is a narrow region,  $\sim 35$  arcmins across, which makes group finding within the strip itself difficult. For this reason, we first find groups in the SDSS, in a region 2 degrees across and centered on the MGC. We define our SDSS galaxy sample to be directly analogous to the CNOC2 sample. There are two areas of particular relevance to this work where these differ: completeness and depth. Because the SDSS has a much higher completeness ( $\sim 90\%$ ) than the CNOC2 redshift survey ( $\sim 48\%$ ), we randomly remove half the SDSS galaxies. Further, we use the same absolute magnitude cut as Carlberg et al.,  $M_R = -18.5$ , with an additional evolution correction of 1 magnitude per unit redshift.

Carlberg et al.'s primary goal was to find virialized groups in overdense environments, so they estimate the overdensity of each galaxy and restrict their group finding algorithm to galaxies in dense environments. A cylinder of

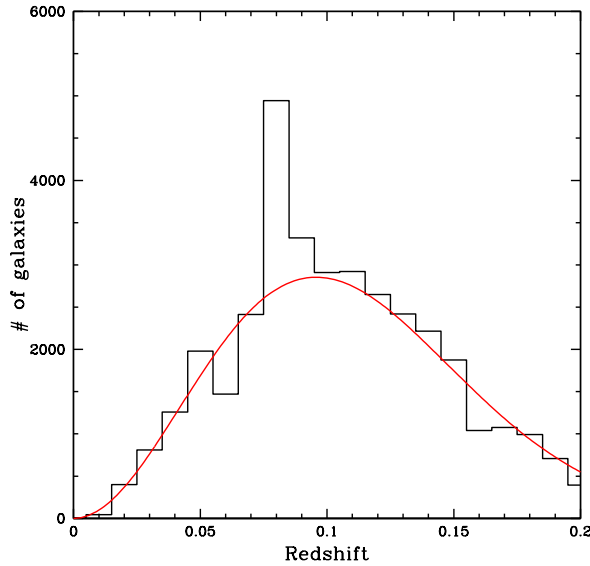


**Figure A1.** The redshift distribution of the full sample of SDSS galaxies which were used to find groups at low redshift. The red line is the Maxwellian fit to the data which was used to estimate the background.

$0.33h_{75}^{-1}$  Mpc radius and  $\pm 6.67h_{75}^{-1}$  Mpc line-of-sight depth is centered around each galaxy and the number of galaxies within the cylinder is counted. If there are fewer than 3 neighbours in this cylinder, the process is repeated with a cylinder 1.5 times larger. A background estimate is then obtained by randomly drawing points from a redshift distribution fit to the entire sample. Figure A1 shows the redshift distribution of galaxies in our sample and our analytic fit. If the number of neighbours in the cylinder is greater than the background estimate then the main galaxy is kept as a possible group member.

Starting with the galaxy with the greatest overdensity, we begin a trial group by adding any galaxies within the original cylinder, and any of their friends. When we run out of friends we have a trial group, for which the geometric position, redshift and velocity dispersion are computed. Galaxies are trimmed or added within  $1.5R_{200}$  and three velocity dispersions, where  $R_{200}$  is the radius at which the density is 200 times the critical density. This process is iterated four times with the requirement that the last two iterations are identical. A group is moved to the next stage if it has more than two members. This concludes the Carlberg et al. algorithm.

The next stage is to emulate the process in Wilman et al. (2005b), to account for the targeted spectroscopic follow-up, which resulted in a more nearly complete redshift sampling around selected groups. We do this by including the complete SDSS catalogue. We use the Carlberg initial centres but set the velocity dispersion equal to 500 km/s, as was done by Wilman et al. This was done to remove any bias in the starting velocity dispersions, which were only based on very few galaxies. We again iterate on these positions using the entire SDSS catalogue and recompute the luminosity weighted centres. We compute the velocity dispersion at each step using the Gapper estimator and remove galaxies outside two velocity dispersions and  $500h_{75}^{-1}$  kpc. Fi-

nally, we keep only those groups which lie completely within the MGC strip. Using this method we have 19 groups with velocity dispersions between 100 km/s and 700 km/s, and which lie within  $0.04 < z < 0.12$ .

There exist a large number of group and cluster catalogues based on the SDSS and 2DF surveys with which we can compare. This is especially important to calibrate the systematic effects which may be present in our high redshift sample, which doesn't have sufficient completeness to quantify within the survey itself. One of the more popular group finding algorithms, and the most direct analogue to our method, is that of Berlind et al. (2006). They use a traditional friends-of-friends algorithm in position-redshift space to find groups in three different volume limited samples. We find that 12 out of 13 of our groups below  $z=0.1$ , the depth of the deepest Berlind sample, are also found in the Berlind catalogue, ie. the Berlind group centres are contained within our groups. Eighty-five of the 99 group members which make up the low redshift group sample in this paper would also be group members if we were to use the Berlind catalogue as our group catalogue.

## APPENDIX B: DEPENDENCE OF GALAXY PROPERTIES ON PSF SIZE

As discussed in §2.3, the CNOC2 and MGC surveys compare well in absolute surface brightness limits, physical size of the PSF and the rest waveband used in the morphological decomposition. In fact, the biggest variation in these parameters is actually within the MGC sample itself. The PSF size is  $\sim 3$  kpc in size at  $z = 0.14$  and just  $\sim 1$  kpc at  $z=0.05$ .

In this section, we investigate the redshift dependence of the key morphological indicators in three bins of redshift within the MGC sample. Some care must be taken because, as we have seen, the disk fraction changes rapidly with luminosity; therefore, without first matching on luminosity we would have a higher disk fraction in the lowest redshift bins. We have broken the sample into low ( $0 < z \leq 0.05$ ), medium ( $0.05 < z \leq 0.1$ ) and high ( $0.1 < z \leq 0.15$ ) redshift bins. Each galaxy in the  $0.05 < z \leq 0.1$  bin was randomly matched to a galaxy in each of the other two redshift ranges with an absolute B magnitude within 0.03 magnitudes. The sample has 2169 galaxies in the  $0.05 < z < 0.1$  range. They were matched to a unique sample of 266 galaxies in the  $0 < z < 0.05$  range and 1354 galaxies in the  $0.1 < z < 0.15$  range. Each galaxy was weighted by the number of times it was matched.

Figure B1 shows the B/T distribution of the three different redshift samples. These distributions are very similar in all redshift bins and our conclusions are unchanged if the field sample is taken as any of these bins.

In §3.3, we claim that the observed difference in the mean asymmetries between the CNOC2 sample and the MGC sample is due to the better physical resolution of the CNOC2 images. To test this we reduce the resolution of the original image and the residual image of a representative sample of 60 galaxies from our CNOC2 sample by convolving with a Gaussian with different widths. Figure B2 shows the asymmetry distribution of the original sample (thin, solid black line), and the asymmetries after broadening with a 1 kpc (black, dashed line) and 2 kpc PSF (thick, solid black

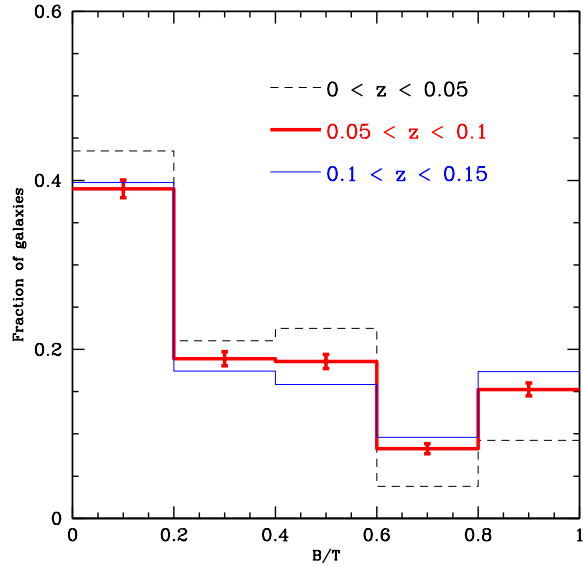


**Figure B1.** The B/T distribution of luminosity-matched samples of MGC galaxies in bins of redshift. The sample is divided into low ( $0 < z < 0.05$ ; thin, dashed, black line), medium ( $0.05 < z < 0.1$ ; thick red line) and high ( $0.1 < z < 0.15$ ; thin, solid, blue line) redshift bins

line). Clearly the asymmetry is reduced with poorer physical resolution, which explains the higher asymmetries of the CNOC2 sample. For this reason, we do not compare the asymmetries between the two surveys and always use samples matched in redshift within a given survey.

## APPENDIX C: IMAGES OF A SAMPLE OF GROUP AND FIELD GALAXIES AT Z=0.4

In this section, we show a representative sample of the group and field galaxies from our CNOC2  $z=0.4$  sample. As discussed in §2.3, the thumbnail images are from *HST* ACS observations. Each image is shown together with the GIM2D model and the residual of the *HST* image after the model was removed. We show the group galaxies in Figure C1, and the field galaxies in Figure C2. In Figure C3, we show images of the nine group galaxies in the CNOC2 sample which are bulge dominated ( $B/T > 0.5$ ) and have high asymmetries ( $R_T + R_A > 0.16$ ). The first four of these galaxies show interaction features.

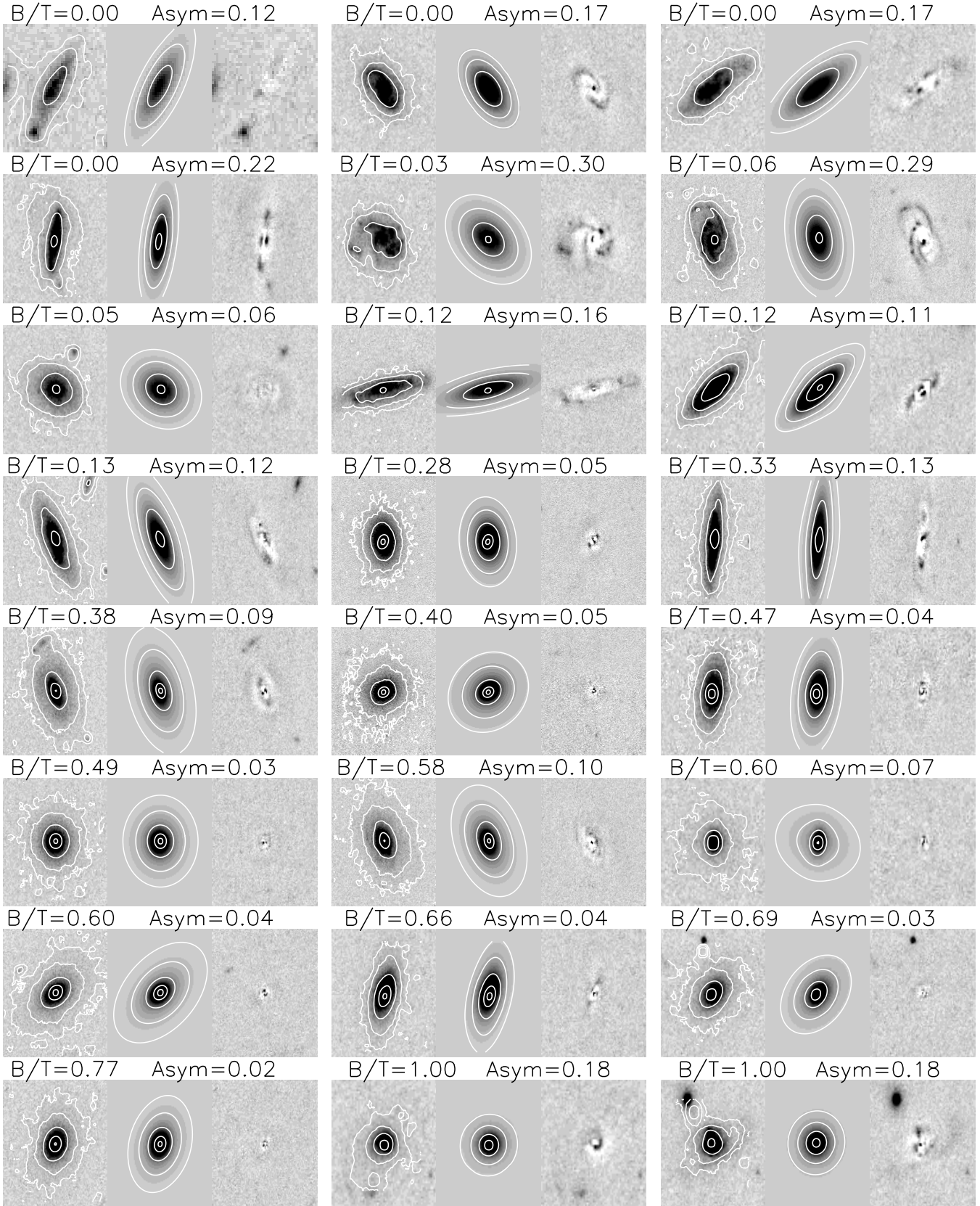


**Figure C1.** A representative sample of group galaxy images from the  $z=0.4$  sample. For each of 24 galaxies is the *HST* ACS image (left panel), the GIM2D output model galaxy (middle panel), and the residual of the *HST* ACS image after the model is subtracted (right panel). Each galaxy is listed with the Bulge to total ratio ( $B/T$ ) and Asymmetry (Asym) computed by GIM2D.

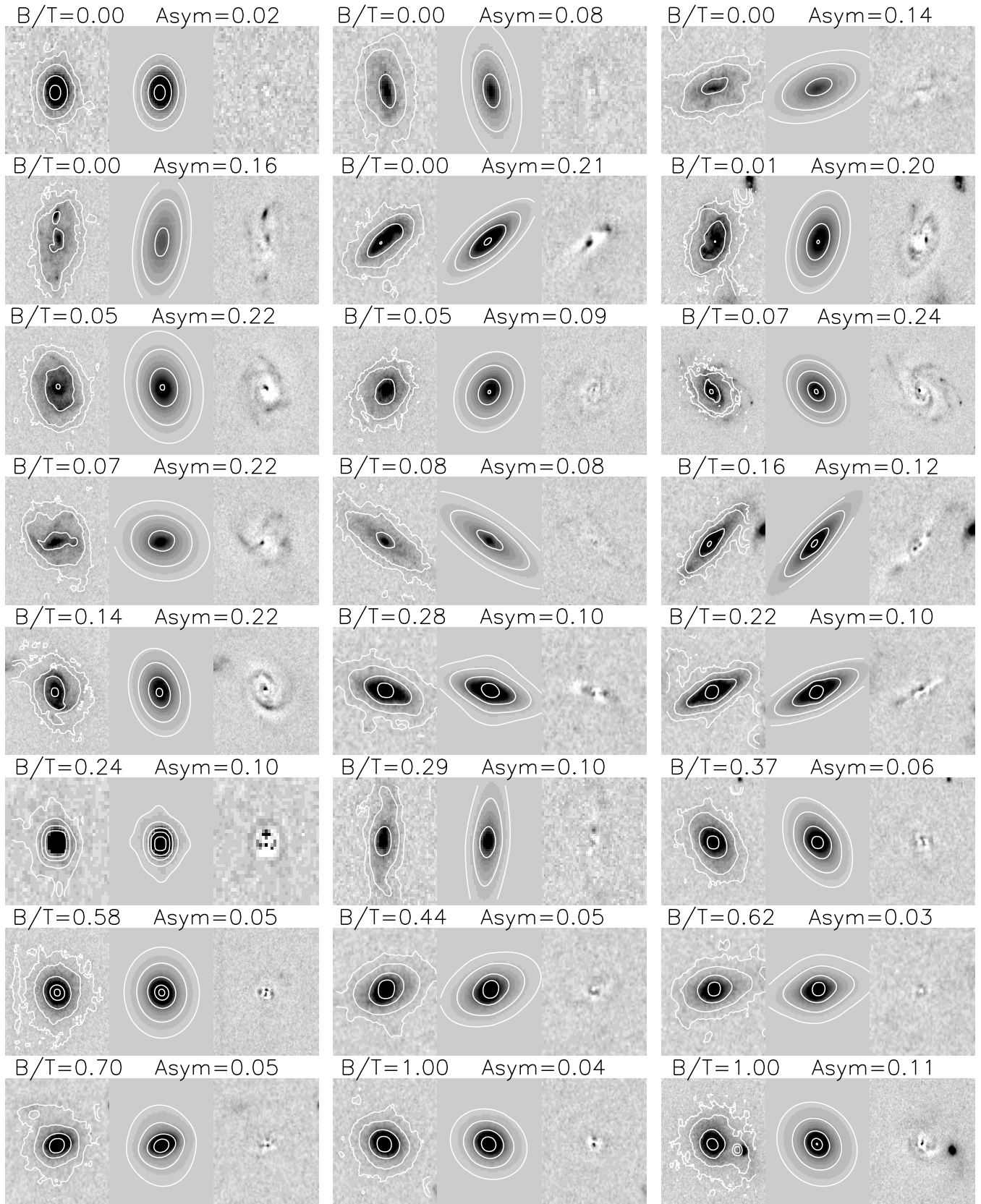


**Figure C2.** As in Figure C1, but for a representative sample of 24 field galaxies in the  $z=0.4$  sample.

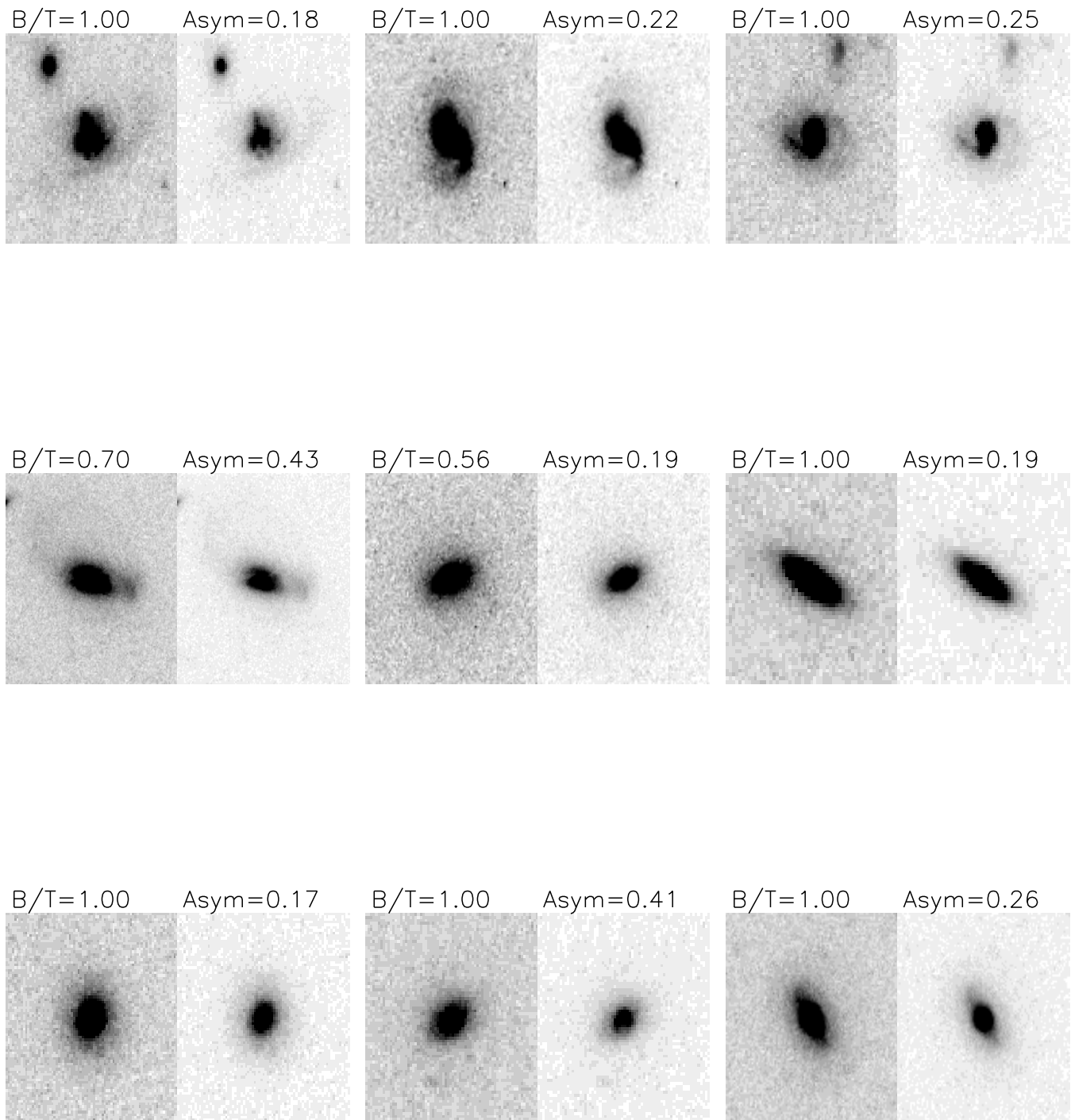


**Figure C3.** The nine group galaxies in the  $z=0.4$  sample which are bulge dominated ( $B/T > 0.5$ ) and highly asymmetric ( $R_T + R_A > 0.16$ ). The galaxies are shown with two stretches to show the interaction features. Prominent interaction features are seen in the first four of these galaxies.

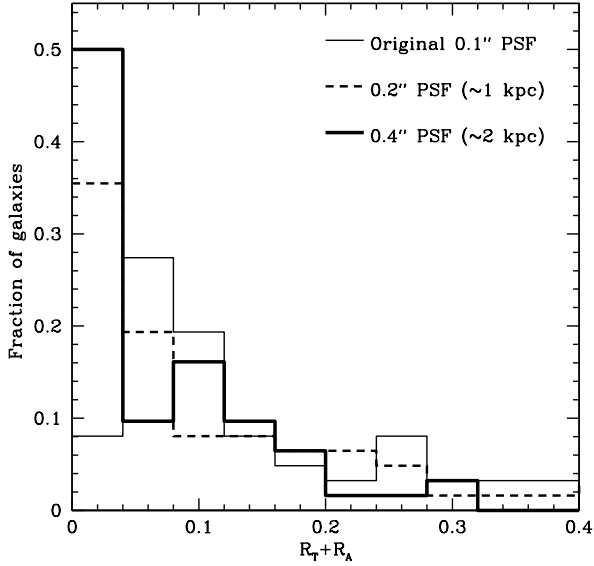


**Figure B2.** The distribution of asymmetries ( $R_T + R_A$ ) measured within 2 halfflight radii for different physical resolutions for a sample of 60 representative CNOC2 galaxies. The images were blurred with a Gaussian with a PSF of 1 (black, dashed line) and 2 kpc (thick, solid black line). The original, unblurred asymmetry is shown as the thin black line.